NTNU
Norwegian University of
Science and Technology

Schrödinger-Poisson and nonequilibrium Green's function methods applied to layered semiconductor devices

Mikael Haug

Master of Science in Physics and Mathematics
Submission date: June 2018
Supervisor: Jon Andreas Støvneng, IFY
Co-supervisor: Trond Brudevoll, FFI
Asta-Katrine Storebø, FFI

Norwegian University of Science and Technology
Department of Physics

Abstract

In this work, electron transport through layered semiconductor heterostructure devices in the nanometer dimension are simulated. Because these devices have shrunk in the last decades, it is no longer sufficient to utilize only semiclassical transport theory. This is because it neglects quantum mechanical effects such as tunneling, interference and confinement. Thus, the need for a fully quantum mechanical corrected theory arises. The application for these devices range range within the fields of nanoelectronics, optoelectronics and flexible or stretchable electronic devices. Both of the methods are compared; the semiclassical theory uses a Schrödinger-Poisson solver, and the fully quantum mechanical theory uses a nonequilibrium Green's function method. Both methods are studied in one dimension for electron transport, in the singleband approximation. Since there are spatial charges throughout the device, these will affect the shape of the electric potential profile. So, the Schrödinger-Poisson solver first calculates the quantum mechanical states from the Schrödinger equation, with an initial ansatz for the potential profile. Then, the states that are obtained are substituted into the Poisson equation, which takes into account spatial charges and calculates a new potential profile. The profile is substituted into the Schrödinger equation again, and the process is iteratively repeated. The problem is that one must make an assumption for the electron density involved in the Poisson equation, which does not take into account inelastic scattering effects of the electrons. In the nonequilibrium Green's function case, the same ansatz for the potential profile is used. Once the Green's functions have been calculated, the electron density may be obtained and substituted into the Poisson equation for calculations of a new profile. The resulting profile obtained is substituted into the Green's function equations, and the process is iteratively repeated. The result is that the less accurate but more rapid semiclassical approach is traded off for a much slower but simultaneously more accurate fully quantum mechanical theory.

Preface

This report was submitted in the academic semester in the summer of 2018 for the Department of Physics at Norges Teknisk-Naturvitenskapelige Universitet in cooperation with Forsvarets Forskningsinstitutt. The present work treats one-dimensional electron transport in layered structures using semiclassical and quantum mechanical transport theory, and is presumed to be read by those who already have preliminary knowledge of these subjects.

Acknowledgements

I would like to thank everyone who has contributed to this work for the past ten months. This includes my supervisors Trond Brudevoll, Asta-Katrine Storebø and co-supervisor Jon Andreas Støvneng. I would like to thank my supervisors for providing me with great amounts of information related to this work, and my co-supervisor on how to structure this report.

I would also like to thank Christian Jirauschek for providing me with a few examples, and for helping me understand some of the implementation of the advanced equations and methods that are involved in this work.

There were numerous times where I was ready to admit defeat, but as Trond Brudevoll motivatingly enunciated (and I paraphrase): ”Whenever you feel down, remember that nonequilibrium Green’s functions will always put a smile on your face.”

Table of Contents

List of Tables

List of Figures

Abbreviations

NEGF	=	Nonequilibrium Green's function
GF	=	Green's function
SP	=	Schrödinger-Poisson
FDM	=	Finite Difference Method
RTD	=	Resonant Tunneling Diode
laser	=	Light Amplification by Stimulated Emission of Radiation
QCL	=	Quantum Cascade Laser
QCD	=	Quantum Cascade Detector

Chapter 1

Introduction

1.1 Background

In the middle of the 20th century, semiconductors were at the frontier of new technological developments within the field of solid state physics (Shockley, 1950). Semiconductor devices operate on the basis of controlling flow of electrons and holes through the device. These particles were treated in the semiclassical regime with an effective mass, which at that time was adequate. The semiclassical transport theory is based on quantum mechanical principles, but quantum effects such as tunneling, interference and confinement are neglected. Properties such as effective mass and bandgaps could be looked up easily for these semiconductors. However, more recently in the 21st century, the semiconductor devices have shrunk to the nanoscale regime. Consequently, these devices can be engineered so that desired properties emerge. In order to describe these devices, it is necessary to think about charge carriers as quantum mechanical properties rather than as semiclassical particles (M. P. Anantram and Nikonov, 2008). The applications for these semiconductor devices are plenty, from nanoelectronics and optoelectronics to flexible devices. From devices such as quantum cascade lasers (QCL) (J. Faist and Cho, 1994) and detectors (QCD) (D. Hofstetter and Köhler, 2010), to thermoelectric devices and biomedical ablation (Hashimura et al., 2014), (Ming-Yang Li and Li, 2008).

1.2 Motivation and structure of the report

The purpose of this present work is to show preliminary results for the semi-classical Schrödinger-Poisson (SP) method, and compare this with the fully quantum mechanical nonequilibrium Green's function approach (NEGF). The SP method is efficient and fast, but this is traded off with a lot slower and more accurate results in the NEGF approach. The slow computational time for NEGF still remains a challenge today, and the author is motivated to improve on this issue. Here, only electrons are treated within the single-band band one dimensional approximation.

There exists numerous techniques in order to simulate the layered semiconductor device. Some are based on empirical approaches, which means that experimental data such as transition rates between relevant energy levels are used as input. Others are self-consistent, which means that they only rely on well known material properties such as effective mass. But they do not rely on experimental values for transition rates.

Semiclassical	Quantum transport
Empirical	
Rate equations	1D density matrix
Maxwell-Bloch	
Self-consistent	
Rate equations	1D/3D density matrix
Monte Carlo	NEGF

Table 1.1: Carrier transport techniques for layered semiconductor structure simulations.

The rate equations are based upon the transition rates between energy levels, which are either empirically documented or self-consistently solved. The Maxwell-Bloch equations are generalizations of the rate equations, however optical fields are modeled using density matrices instead of scattering rates. Similarly, in quantum mechanics the density matrix is also used as generalization of the rate equations, but it includes quantum effects such as tunneling and dephasing. These methods will not be discussed further in this work.

In this work the Finite Difference Method (FDM) will be used, and will be covered in section 2.7 and used in section 3.1. The report covers

fundamental aspects in semiclassical as well as fully quantum mechanical transport theory in chapter 2. Further on in chapter 3, the numerical implementation of the SP and NEGF methods will be discussed in detail. Results of the simulations are given in chapter 4, and the report ends with concluding remarks and further outlook in chapter 5.

Chapter 2

Theory

2.1 Preliminaries

This chapter begins by briefly explaining a few concepts which are considered as the basis for understanding the Schrödinger-Poisson equations and the NEGF theory handled later on.

2.1.1 Bloch states

Since a crystal has a structure which repeats itself in all directions, the potential energy will be periodic. The Schrödinger equation for an electron can be written as

$$\Big[\frac{-\hbar^2}{2m}\nabla^2 + U(\boldsymbol{r})\Big]\psi(\boldsymbol{r}) = E\psi(\boldsymbol{r}), \tag{2.1}$$

where the potential $U(\boldsymbol{r})$ has the periodicity

$$U(\boldsymbol{r}) = U(\boldsymbol{r} + \boldsymbol{R}). \tag{2.2}$$

Here, $\boldsymbol{R}$ is a direct lattice vector. The general solution of this equation is given by

$$\psi_{\boldsymbol{k}}(\boldsymbol{r}) = \mathrm{e}^{i\boldsymbol{k}\cdot\boldsymbol{r}} u_{\boldsymbol{k}}(\boldsymbol{r}), \tag{2.3}$$

where the function $u_{\boldsymbol{k}}(\boldsymbol{r}) = u_{\boldsymbol{k}}(\boldsymbol{r} + \boldsymbol{R})$. It immediately follows that the probability distribution is the same for every repetition of the lattice $\big|\psi(\boldsymbol{r} +$

$\boldsymbol{R})\big|^2 = \big|\psi(\boldsymbol{r})\big|^2$.

2.1.2 $\boldsymbol{k}\cdot\boldsymbol{p}$ method

This is a method used to calculate effective mass for particles moving in a crystal. Because of the potential of the crystal, the particles behave as if they have a different mass than they would have in vacuum (Singh, 2003, p. 74). The approximation only holds for $\boldsymbol{k}$ values close to the conduction band edge (Singh, 2003, p. 76).

The function $u_{n,\boldsymbol{k}_0}(\boldsymbol{r})$ of the Bloch state from Equation 2.3 in energy level n will in perturbation theory satisfy the Schrödinger equation

$$H_{\boldsymbol{k}} u_{n,\boldsymbol{k}_0}(\boldsymbol{r}) = E_{n,\boldsymbol{k}_0} u_{n,\boldsymbol{k}_0}(\boldsymbol{r}), \tag{2.4}$$

where the Hamiltonian $H = H_0 + H'$ with H' as the perturbative term and setting $\boldsymbol{k}_0 = 0$. In $\boldsymbol{k}\cdot\boldsymbol{p}$ theory, the perturbative part can be expressed as

$$H' = \frac{\hbar^2 k^2}{2m} + \frac{\hbar \boldsymbol{k}\cdot\boldsymbol{p}}{m}. \tag{2.5}$$

The known part is given by Equation 2.1. In the conduction band, the eigenenergy can be approximated as

$$E_c(\boldsymbol{k}) \approx E_{c,\boldsymbol{k}_0} + \frac{\hbar^2 k^2}{2m} + \frac{\hbar^2}{E_g m^2} \sum_n \big|\big\langle u_{c,\boldsymbol{k}_0}\big|\boldsymbol{k}\cdot\boldsymbol{p}\big|u_{c,\boldsymbol{k}_0}\big\rangle\big|^2, \tag{2.6}$$

where E_g is the band gap energy between the minimum of the conduction and the maximum of the valence band.

The energy will take parabolic forms such as a spherical form, ellipsoidal or warped (Jacoboni, 2010, p. 118). The different types of effective masses can be obtained by taking the derivative of the energy E_c with respect to $\boldsymbol{k}$.

2.1.3 Quantum mechanical formulations

There are three main quantum mechanical formulations a system may be described by, and all of them are equivalent (Shafer, 2009). They are named the Schrödinger, Heisenberg and interaction pictures, with the respective subscripts S, H and I It should be understood that the Hamiltonian is here in the Schrödinger picture. The three pictures are described below.

Schrödinger picture

In this picture, the states are time-dependent, but the observables are constant. This gives the relations

$$\big|\psi_S(t)\big\rangle = U(t,t_0)\big|\psi_S(t_0)\big\rangle, \tag{2.7}$$

where $U(t,t_0)$ is the time evolution operator, and has the interpretation that it evolves a state from time t_0 to t.

Heisenberg picture

Here the states are constant, instead the observables propagate in time. Suppose that the Hamiltonian is time-independent, then the time evolution operator can be written as

$$U(t,t_0) = \mathrm{e}^{-iH(t-t_0)/\hbar}. \tag{2.8}$$

Then, the expectation value for an operator, A_S for the state $\big|\psi_H(t_0)\big\rangle$ becomes

$$\big\langle A_S\big\rangle_t = \big\langle\psi_H(t_0 0)\big|A_H(t)\big|\psi_H(t_0)\big\rangle, \tag{2.9}$$

where $A_H(t) \equiv \mathrm{e}^{iH(t-t_0)/\hbar}A_S\mathrm{e}^{-iH(t-t_0)/\hbar}$.

Interaction picture

For systems which experience a perturbation, the Hamiltonian is usually split into one part of which the solution of the Schrödinger equation is known (H_0) and one perturbative (H_I) term

$$H = H_0 + H_I. \tag{2.10}$$

The states are defined as

$$\big|\psi_I(t)\big\rangle \equiv \mathrm{e}^{iH_0t/\hbar}\big|\psi_S(t)\big\rangle. \tag{2.11}$$

The operators are time-dependent, and are defined as

$$A_I(t) = \mathrm{e}^{iH_0t/\hbar}A_S\mathrm{e}^{-iH_0t/\hbar}. \tag{2.12}$$

This last picture is the one which will be used later on.

2.1.4 Time ordering operator

For two time dependent operators, $A(t)$ and $B(t')$ at different times $t \neq t'$ the time ordering operator, T acting on the product of these two is defined such that

$$T[A(t)B(t')] = \begin{cases} A(t)B(t') & \text{if } t > t' \\ B(t')A(t) & \text{if } t' > t \end{cases} \tag{2.13}$$

An equivalent formulation is one using the unit step function, $\theta(t)$

$$T[A(t)B(t')] = A(t)B(t')\theta(t-t') \pm B(t')A(t)\theta(t'-t), \tag{2.14}$$

with $+$ for Bosons and $-$ for Fermions.

2.2 Scattering

There exists numerous scattering processes, and these must be taken into account for the electrons traveling in the system. The processes of most importance are lattice vibrations or phonons, electron interaction with impurities such as ionized donors, interface roughness, alloy disorders, and electron interactions among themselves (Franckié, 2016, p. 24). The details of these processes will be discussed in this section.

2.2.1 Phonons

In this process, it is assumed that the lattice is not deformed, but rather displaced. This can be described by a displacement field $\boldsymbol{y}(\boldsymbol{r}, t)$ so that the perturbed Hamiltonian becomes (Jacoboni, 2010, p. 132)

$$H' = \sum_{ij} E_{ij} \frac{\partial y_i}{\partial y_j}, \tag{2.15}$$

where E_{ij} is a deformation-potential tensor constant. In the case of acoustic phonons, the deformation constant is a third rank tensor constant. The most general expression for small vibrations of a chain in three dimensions is

$$\boldsymbol{y}_j(\boldsymbol{r},t) = \sum_{\boldsymbol{q},l} \boldsymbol{e}_{\boldsymbol{q},l}\Big\{\xi_{\boldsymbol{q},l}\mathrm{e}^{i(\boldsymbol{q}\cdot\boldsymbol{r}_j-\omega_l(\boldsymbol{q}))t} + \xi^*_{\boldsymbol{q},l}\mathrm{e}^{-i(\boldsymbol{q}\cdot\boldsymbol{r}_j-\omega_l(\boldsymbol{q}))t}\Big\}, \tag{2.16}$$

where $\boldsymbol{e}_{\boldsymbol{q},l}$ is the polarization vector for a given wavevector $\boldsymbol{q}$ and mode l, and $\xi_{\boldsymbol{q},l}$ is the amplitude of the displacement. By using normal coordinates and expressing the displacement field in second quantization, one obtains

$$\boldsymbol{y}_j(\boldsymbol{r},t) = \sum_{\boldsymbol{q},l} \boldsymbol{e}_{\boldsymbol{q},l}\left(\frac{\hbar}{2\rho V\omega_l(\boldsymbol{q})}\right)^{1/2}\Big\{\mathrm{a}_{\boldsymbol{q},l} + \mathrm{a}^\dagger_{-\boldsymbol{q},l}\Big\}\mathrm{e}^{i\boldsymbol{q}\cdot\boldsymbol{r}}. \tag{2.17}$$

Thus the perturbed Hamiltonian becomes

$$H' = \sum_{ij} E_{ij}\sum_{\boldsymbol{q},l}[\boldsymbol{e}_{\boldsymbol{q},l}]_i i q_j\left(\frac{\hbar}{2\rho V\omega_l(\boldsymbol{q})}\right)^{1/2}\Big\{\mathrm{a}_{\boldsymbol{q},l} + \mathrm{a}^\dagger_{-\boldsymbol{q},l}\Big\}\mathrm{e}^{i\boldsymbol{q}\cdot\boldsymbol{r}}. \tag{2.18}$$

2.2.2 Impurities

These are either charged or neutral particles, and respectively interact with electrons in a long or short range. Neutral impurities will not be discussed here, as it assumes slowly moving electrons.

The charged impurities can be treated by Coulomb interactions, and usually the Brooks Herring approach (Jacoboni, 2010, p. 153) is used by introducing a screening effect

$$V(\boldsymbol{r}) = \frac{Ze(-e)}{4\pi\epsilon r}\mathrm{e}^{-q_0 r}. \tag{2.19}$$

Here, Z is the atom number for the impurity, r is the distance between the electron and the impurity, ϵ is the dielectric constant and q_0 is the inverse screening length.

2.2.3 Alloy scattering

The layered device consists of a mixture or alloy of different materials. Because of this, there will be a perturbation which allows transitions between Bloch states.

Suppose the material consists of an alloy with a fraction x of material A, and a corresponding fraction $(1 - x)$ of material B. Then, a virtual potential arises which can be written as (Jacoboni, 2010, p. 158)

$$V_v = xV_A + (1 - x)V_B, \tag{2.20}$$

where V_A and V_B are the respective potentials because of atom A and B, and V_v is the resulting virtual potential.

Because of inconsistencies in the material, a site which for instance should be occupied by atom A may instead be occupied by atom B, and vice versa. This is what causes perturbation and thus scattering. The probability of finding the "wrong atom" is then given by the probability that atom A is supposed to be in that site multiplied by the probability that atom B is actually located there. The opposite case is added to this effect. The resulting probability density can then be written as

$$n = 2\frac{1}{V_c}x(1 - x), \tag{2.21}$$

where V_c is the volume of the unit cell of the crystal.

2.2.4 Electron-electron interactions

It is necessary to have knowledge about the distribution of the electrons in the material in order to include electron-electron interaction. This is because Coulomb interaction must be included, as well as the probability that an electron with momentum $\boldsymbol{k}$ will interact with another electron with momentum $\boldsymbol{k}'$.

2.2.5 Interface roughness scattering

When two materials are put together, the interface between them will never be perfectly smooth. This roughness can be described as a potential for the electrons. This potential will depend upon a small deviation probability, here called $\eta(\boldsymbol{r})$ with spatial dependence. The deviation describes how much the interface between the two materials deviate from a straight line, as they are supposed to be completely flat.

The interface roughness potential is averaged over the deviations, which leads to evaluation of the correlation function $\big\langle \eta(\boldsymbol{r})\eta(0) \big\rangle$. One may choose

a Gaussian or an exponential distribution (Franckié, 2016, p. 26). For instance, the Gaussian is given by

$$\langle \eta(\boldsymbol{r})\eta(0)\rangle = \Delta^2 \exp\left(-\frac{|\boldsymbol{r}|^2}{\Lambda^2}\right), \tag{2.22}$$

where Δ is an average depth or height of a roughness, and Λ the length.

2.3 Resonant tunneling diodes

This type of diode is structured with one layer of high-mobility semiconductor material such as GaAs, and a layer of another high-moobility semiconductor material with higher potential energy in comparison with GaAs such as AlGaAs (Jacoboni, 2010, p. 427). A multiple quantum well/barrier structure can be formed with this method of alternating the material of each layer.

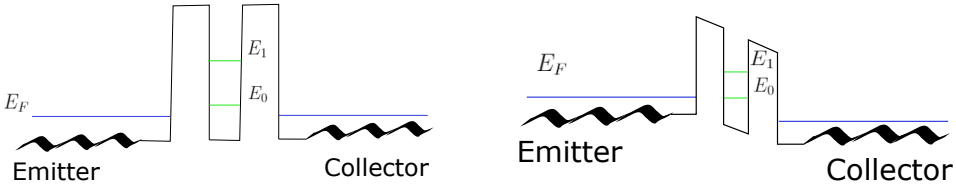

(a) No applied bias. **(b)** Applied voltage bias $V > 0$.

Figure 2.1: A simple resonant tunneling diode consisting here of two resonant energies E_0 and E_1 with electrons filled up to the Fermi energy, E_F in both the emitter and collector regions in Figure 2.1a. When a voltage is applied, the Fermi energy aligns with the resonant energy E_0 which allows for quantum tunneling through the RTD.

When a bias is applied to the resonant tunneling diode (RTD), the potential profile will linearly decrease as shown in Figure 2.1b. Note that the conduction profile of the RTD will lay below the Fermi energy of the electrons, otherwise no electrons could occupy those areas. Electrons accumulate in the emitter region, tunnel through and fill up the Fermi energy in the collector region. However, because of the applied bias these electrons will be depleted, and new electrons are emitted again in the left reservoir. As the applied bias is increased even more, the resonant states will misalign with

the Fermi level. This means that the current will decrease, until it aligns with the next resonant energy level in the RTD where it increases again. So one expects to find current peaks for increased biases.

2.4 Many-particle systems

Going from a single particle to multiple or many-particle systems, the eigenstates have to be revised so they include all particles in every possible state.

2.4.1 Field operators

For a state with multiple particles, the annihilation operator for particle k for Bosons acting on the state gives

$$\mathrm{a}_k\big|n_1, n_2, ..., n_k, ...\big\rangle = \sqrt{n_k}\big|n_1, n_2, ..., n_k - 1, ...\big\rangle, \tag{2.23}$$

while the creation operator gives

$$\mathrm{a}_k^\dagger\big|n_1, n_2, ..., n_k, ...\big\rangle = \sqrt{n_k + 1}\big|n_1, n_2, ..., n_k + 1, ...\big\rangle. \tag{2.24}$$

Because of the antisymmetric properties of Fermion states, only one Fermion can occupy a given state. This condition gives the following result for the annihilation operator acting on a state

$$\mathrm{b}_k\big|n_1, n_2, ..., n_k, ...\big\rangle = \begin{cases} (-1)^{S_k}\big|n_1, n_2, ..., n_k - 1, ...\big\rangle & \text{if } n_k = 1 \\ 0 & \text{if } n_k = 0 \end{cases} \tag{2.25}$$

where $S_k = n_1 + n_2 + ... + n_{k-1}$ is the number of states before reaching state k, and takes into account the antisymmetry property of Fermion states. Similarily for the creation operator

$$\mathrm{b}_k^\dagger\big|n_1, n_2, ..., n_k, ...\big\rangle = \begin{cases} (-1)^{S_k}\big|n_1, n_2, ..., n_k + 1, ...\big\rangle & \text{if } n_k = 0 \\ 0 & \text{if } n_k = 1 \end{cases} \tag{2.26}$$

The general commutation relations for the operators can be summed up as

$$[\mathrm{c}_k, \mathrm{c}_{k'}^\dagger]_\mp = \delta_{kk'} \qquad [\mathrm{c}_k, \mathrm{c}_{k'}]_\mp = [\mathrm{c}_k^\dagger, \mathrm{c}_{k'}^\dagger]_\mp = 0, \tag{2.27}$$

where c is either a bosonic or fermionic annihilation operator, and the upper and lower sign respectively accounts for the bosonic and fermionic cases.

Given a complete set of single-particle states $\psi(\boldsymbol{r})$, field operators may be defined as

$$\Psi(\boldsymbol{r}) = \sum_k \psi_k(\boldsymbol{r}) c_k, \qquad \Psi^\dagger = \sum_k \psi_k^*(\boldsymbol{r}) c_k^\dagger, \tag{2.28}$$

with properties following from 2.27 and the spatial normalization of $\psi(\boldsymbol{r})$

$$[\Psi(\boldsymbol{r}), \Psi^\dagger(\boldsymbol{r}')]_\mp = \delta(\boldsymbol{r} - \boldsymbol{r}') \qquad [\Psi(\boldsymbol{r}), \Psi(\boldsymbol{r}')]_\mp = [\Psi^\dagger, \Psi^\dagger]_\mp = 0. \tag{2.29}$$

The field operators may also be time-dependent, in which case the time evolution in the Heisenberg picture may be embedded into c as the states are constant in time,

$$\Psi(\boldsymbol{r}, t) = \sum_k \psi_k(\boldsymbol{r}) c_k(t), \qquad \Psi^\dagger = \sum_k \psi_k^*(\boldsymbol{r}) c_k^\dagger(t). \tag{2.30}$$

2.4.2 Second quantization of operators

For a single-particle operator A, in its position representation it can be expressed as

$$A = \sum_i a(r_i) \tag{2.31}$$

in its second quantization it can be expressed as (Jacoboni, 2010, p. 448)

$$A = \sum_{kk'} c_k^\dagger a_{kk'} c_{k'} \tag{2.32}$$

where $a_{kk'} = \langle k | A | k' \rangle$ for a single-particle state $|k\rangle$. Expressed by the field operators, this becomes

$$A = \int\int \Psi^\dagger(\boldsymbol{r}) A(\boldsymbol{r}, \boldsymbol{r}') \Psi(\boldsymbol{r}') \mathrm{d}\boldsymbol{r} \mathrm{d}\boldsymbol{r}'. \tag{2.33}$$

In the same way, two-particle operators such as a potential in its position representation can be expressed as

$$V = \frac{1}{2}\sum_{i\neq j} v(\boldsymbol{r}_i, \boldsymbol{r}_j), \tag{2.34}$$

where $v(\boldsymbol{r_i}, \boldsymbol{r_j})$ is a two-body spatial potential. In second quantization, it becomes

$$V = \frac{1}{2}\sum_{k,k',k'',k'''} c_k^\dagger c_{k'}^\dagger \big\langle k, k' \big| v \big| k'', k''' \big\rangle c_{k'''} c_{k''}. \tag{2.35}$$

Expressed by the field operators this becomes

$$V = \frac{1}{2}\int\int \Psi^\dagger(\boldsymbol{r})\Psi^\dagger(\boldsymbol{r}')v\Psi(\boldsymbol{r})\Psi(\boldsymbol{r}')\mathrm{d}\boldsymbol{r}\mathrm{d}\boldsymbol{r}'. \tag{2.36}$$

2.4.3 Wick-Matsubara theorem

When treating Green's functions (GF), it will be necessary to evaluate expressions such as

$$\big\langle \Psi^\dagger(\boldsymbol{r}_1, t_1)\Psi(\boldsymbol{r}_2, t_2)\Psi^\dagger(\boldsymbol{r}_3, t_3)\Psi(\boldsymbol{r}_4, t_4)\big\rangle. \tag{2.37}$$

In this case, the expression is evaluated in the interaction picture on a statistical ensemble at equilibrium

$$\big\langle A(t_a)B(t_b)...\big\rangle = \frac{1}{Z}\mathrm{Tr}\big\{\mathrm{e}^{-\beta H_0}A(t_a)B(t_b)...\big\}. \tag{2.38}$$

Here, $A(t_a)B(t_b)...$ are operators, Z is the partitioning function for the ensemble, H_0 is the unperturbed Hamiltonian and $\beta = 1/(k_B T)$ where k_B is Boltzmann's constant and T is the temperature. Substitute the time-dependent expressions for the states to obtain

$$\begin{aligned} &\big\langle \Psi^\dagger(\boldsymbol{r}_1, t_1)\Psi(\boldsymbol{r}_2, t_2)\Psi^\dagger(\boldsymbol{r}_3, t_3)\Psi(\boldsymbol{r}_4, t_4)\big\rangle \\ &= \sum_{\lambda\mu\nu\gamma} \mathrm{e}^{i\omega_\lambda(t_1-t_0)}\mathrm{e}^{i\omega_\mu(t_2-t_0)}\mathrm{e}^{i\omega_\nu(t_3-t_0)}\mathrm{e}^{i\omega_\gamma(t_4-t_0)} \\ &\quad\times\psi_\lambda^*(\boldsymbol{r}_1)\psi_\mu(\boldsymbol{r}_2)\psi_\nu^*(\boldsymbol{r}_3)\psi_\gamma(\boldsymbol{r}_4)\big\langle c_\lambda^\dagger c_\mu c_\nu^\dagger c_\gamma\big\rangle. \end{aligned} \tag{2.39}$$

The goal is to express $\langle c_\lambda^\dagger c_\mu c_\nu^\dagger c_\gamma \rangle$ in pairs of each other, which will lead to simpler expressions for the expansion of the GFs.

Start by using the relations in 2.27 which eventually gives

$$\begin{aligned} &c_\lambda^\dagger c_\mu c_\nu^\dagger c_\gamma \\ &\quad = \left[c_\lambda^\dagger, c_\mu\right]_\mp c_\nu^\dagger c_\gamma \pm c_\mu \left[c_\lambda^\dagger, c_\nu^\dagger\right]_\mp c_\gamma + c_\mu c_\nu^\dagger \left[c_\lambda^\dagger, c_\gamma\right]_\mp \pm c_\mu c_\nu^\dagger c_\gamma c_\lambda^\dagger. \end{aligned} \tag{2.40}$$

The average of the last term will be

$$\left\langle c_\mu c_\nu^\dagger c_\gamma c_\lambda^\dagger \right\rangle = \frac{1}{Z}\mathrm{Tr}\left\{\mathrm{e}^{-\beta H_0} c_\mu c_\nu^\dagger c_\gamma c_\lambda^\dagger\right\} = \frac{1}{Z}\mathrm{Tr}\left\{c_\lambda^\dagger \mathrm{e}^{-\beta H_0} c_\mu c_\nu^\dagger c_\gamma\right\}, \tag{2.41}$$

which holds because the trace is cyclic.

Consider the following differential equation

$$\frac{\mathrm{d}}{\mathrm{d}\beta}\left\{\mathrm{e}^{-\beta H_0} c_\lambda^\dagger \mathrm{e}^{\beta H_0}\right\} = \mathrm{e}^{-\beta H_0}\left[c_\lambda^\dagger, H_0\right]\mathrm{e}^{\beta H_0}. \tag{2.42}$$

From 2.32, the unperturbed Hamiltonian in second quantization formalism may be written

$$H_0 = \sum_\sigma c_\sigma^\dagger c_\sigma \hbar\omega_\sigma, \tag{2.43}$$

where $\hbar\omega_\sigma$ is the eigenenergy. The commutator is then

$$\left[c_\lambda^\dagger, H_0\right] = -c_\lambda^\dagger \hbar\omega_\lambda. \tag{2.44}$$

So 2.42 can be writtens as

$$\frac{\mathrm{d}}{\mathrm{d}\beta}\left\{\mathrm{e}^{-\beta H_0} c_\lambda^\dagger \mathrm{e}^{\beta H_0}\right\} = -\left\{\mathrm{e}^{-\beta H_0} c_\lambda^\dagger \mathrm{e}^{\beta H_0}\right\}\hbar\omega_\lambda. \tag{2.45}$$

Solving the integral in the limits $\beta \to 0$ to β gives

$$\left\{\mathrm{e}^{-\beta H_0} c_\lambda^\dagger \mathrm{e}^{\beta H_0}\right\} = c_\lambda^\dagger \mathrm{e}^{-\beta\hbar\omega_\lambda}, \tag{2.46}$$

or

$$\mathrm{e}^{-\beta H_0} c_\lambda^\dagger = c_\lambda^\dagger \mathrm{e}^{-\beta\hbar\omega_\lambda - \beta H_0}. \tag{2.47}$$

Then at last, 2.41 can be written as

$$\left\langle c_\mu c_\nu^\dagger c_\gamma c_\lambda^\dagger \right\rangle = \mathrm{e}^{\beta\hbar\omega_\lambda}\frac{1}{Z}\mathrm{Tr}\left\{\mathrm{e}^{-\beta H_0} c_\lambda^\dagger c_\mu c_\nu^\dagger c_\gamma\right\} = \mathrm{e}^{\beta\hbar\omega_\lambda}\left\langle c_\lambda^\dagger c_\mu c_\nu^\dagger c_\gamma\right\rangle. \tag{2.48}$$

This result can finally be substituted into 2.40, which gives

$$\begin{aligned}\left\langle c_\mu c_\nu^\dagger c_\gamma c_\lambda^\dagger \right\rangle = \frac{1}{1 \mp \mathrm{e}^{\beta\hbar\omega_\lambda}}\Big(&\left[c_\lambda^\dagger, c_\mu\right]_\mp \left\langle c_\nu^\dagger c_\gamma\right\rangle \\ &\pm \left[c_\lambda^\dagger, c_\nu^\dagger\right]_\mp \left\langle c_\mu c_\gamma\right\rangle + \left\langle c_\mu c_\nu^\dagger\right\rangle \left[c_\lambda^\dagger, c_\gamma\right]_\mp\Big)\end{aligned} \tag{2.49}$$

where it should be noted that the commutators are numbers. The same process can be repeated for the averaged operators inside the brackets, and will yield results such as

$$\left\langle c_\mu c_\gamma\right\rangle = \frac{1}{1 \mp \mathrm{e}^{-\beta\hbar\omega_\mu}}\left[c_\mu, c_\gamma\right]_\mp, \tag{2.50}$$

and

$$\left\langle c_\nu^\dagger c_\gamma\right\rangle = \frac{1}{1 \mp \mathrm{e}^{\beta\hbar\omega_\nu}}\left[c_\nu^\dagger, c_\gamma\right]_\mp. \tag{2.51}$$

In the end, the final expression will be

$$\left\langle c_\mu c_\nu^\dagger c_\gamma c_\lambda^\dagger \right\rangle = \left\langle c_\lambda^\dagger c_\mu\right\rangle\left\langle c_\nu^\dagger c_\gamma\right\rangle \pm \left\langle c_\lambda^\dagger c_\nu^\dagger\right\rangle\left\langle c_\mu c_\gamma\right\rangle + \left\langle c_\lambda^\dagger c_\gamma\right\rangle\left\langle c_\mu c_\nu^\dagger\right\rangle. \tag{2.52}$$

Insert this into 2.37, and obtain

$$\begin{aligned}&\left\langle \Psi^\dagger(\boldsymbol{r}_1,t_1)\Psi(\boldsymbol{r}_2,t_2)\Psi^\dagger(\boldsymbol{r}_3,t_3)\Psi(\boldsymbol{r}_4,t_4)\right\rangle \\ &= \left\langle \Psi^\dagger(\boldsymbol{r}_1,t_1)\Psi(\boldsymbol{r}_2,t_2)\right\rangle\left\langle \Psi^\dagger(\boldsymbol{r}_3,t_3)\Psi(\boldsymbol{r}_4,t_4)\right\rangle \\ &\pm\left\langle \Psi^\dagger(\boldsymbol{r}_1,t_1)\Psi^\dagger(\boldsymbol{r}_3,t_3)\right\rangle\left\langle \Psi(\boldsymbol{r}_2,t_2)\Psi(\boldsymbol{r}_4,t_4)\right\rangle \\ &+\left\langle \Psi^\dagger(\boldsymbol{r}_1,t_1)\Psi(\boldsymbol{r}_4,t_4)\right\rangle\left\langle \Psi(\boldsymbol{r}_2,t_2)\Psi^\dagger(\boldsymbol{r}_3,t_3)\right\rangle.\end{aligned} \tag{2.53}$$

This result can be generalized to give the Wick-Matsubara theorem for N operators in a statistical equilibrium ensemble denoted by zero

$$\begin{aligned}\left\langle T\left[A(t_a)B(t_b)...N(t_n)\right]\right\rangle_0 = &\pm\left\langle T\left[AB\right]\right\rangle_0\left\langle T\left[CD\right]\right\rangle_0 \\ &\pm\left\langle T\left[AC\right]\right\rangle_0\left\langle T\left[BD\right]\right\rangle_0 \pm ...,\end{aligned} \tag{2.54}$$

for each pair of operators where the plus sign is for the case of bosons and minus for fermions.

2.5 Schrödinger-Poisson solver

Determining quantized states in a layered structure is crucial in order to develop and model semiconductor devices such as a QCL or a QCD. For instance, the wavelength of the QCL is determined by the upper and lower lower lasing levels. In QCDs, the levels are used to detect radiation. In order to find these states, the stationary Schrödinger equation is first solved. Then, to account for space charge effects, the Poisson equation is solved to yield a new potential. This effect is then substituted into the Schrödinger equation again, and the process is repeated until convergence is reached.

2.5.1 Schrödinger equation

Because the heterostructure is grown by alternating each layer, the conduction band will form quantum wells and barriers. Since the transport theory is treated in one dimension, the growth direction of the crystal will be denoted by the coordinate z. The Schrödinger equation is in this case given by (Jirauschek and Kubis, 2014, p. 011307 - 6)

$$\left[\frac{\hbar^2}{2}\partial_z\frac{1}{m^*(z)}\partial_z + V(z) - E\right]\psi(z) = 0, \tag{2.55}$$

where $m^*(z)$ is the effective mass in the growth direction, $V(z)$ is the potential, and $\psi(z)$ is the wavefunction in the single-band approximation with eigenenergy, E.

2.5.2 Poisson equation

For the layered structure in this work, the Poisson equation is given by (Jirauschek, 2009, p. 1065)

$$\partial_z\left[\epsilon(z)\partial_z\widetilde{V}(z)\right] = -\rho(z), \tag{2.56}$$

where $\epsilon(z)$ is the electric permittivity, $\widetilde{V}(z)$ is the resulting potential due to space charges because of the charge distribution in the device, and $\rho(z)$ is here given by

$$\rho(z) = e\left[N_D(z) - \sum_i \int_{z_0}^{z_0+L} n_i(z)\right], \tag{2.57}$$

where $N_D(z)$ is the density due to positively charged donors, and $n_i(z)$ is the electron density in energy level i which is integrated over one period L of the structure. The latter effect is summed over all energy levels. Note that since only the conduction band is treated, only electrons are included and not holes. The potential which describes the conduction band with an applied bias is given by

$$V_0(z) = V_c - E_b z/L, \tag{2.58}$$

where V_c is the unbiased conduction band profile, and E_b is the applied voltage bias. The total potential for the entire structure is then $V(z) = V_0(z) + \widetilde{V}(z)$. In this particular case, to avoid large computational times one may choose the Fermi-Dirac distribution (Cassan, 2000), (H. Li and Liu, 2008) for the electron density

$$n_i(z) = \frac{m^*(z)}{\pi\hbar^2} k_B T \left|\psi_i(z)\right|^2 \ln\left(1 + \exp\left[\frac{(\mu - \widetilde{E}_i)}{k_B T}\right]\right). \tag{2.59}$$

Here, k_B is the Boltzmann constant, μ is the chemical potential, and $\widetilde{E}_i = E_n - E_b \int z\left|\psi(z)\right|^2 / L \mathrm{d}z$ which takes into account the applied bias.

In order to find the chemical potential, one may assume it to be constant throughout the device. But one may also use the charge neutrality condition over one period of the structure

$$\sum_i \int_{z_0}^{z_0+L} n_i(z)\mathrm{d}z = \int_{z_0}^{z_0+L} N_D(z)\mathrm{d}z \tag{2.60}$$

The chemical potential can then be found by finding an upper limit

$$\sum_i \int_{z_0}^{z_0+L} n_i(z)\mathrm{d}z < \int_{z_0}^{z_0+L} n(z)\mathrm{d}z \tag{2.61}$$

for μ, and then a lower limit

$$\sum_i \int_{z_0}^{z_0+L} n_i(z)\mathrm{d}z > \int_{z_0}^{z_0+L} n(z)\mathrm{d}z \tag{2.62}$$

The chemical potential is then found from this by for instance using the bisection method (Jirauschek and Kubis, 2014, p. 011307 - 10).

2.6 Nonequilibrium Green's function solver

There is a need for a fully quantum mechanical theory when the device structures are of the nanometer scale. Effects such as quantum interference, coherent tunneling and confinement must be appropriately accounted for. Additionally in the mesoscopic regime, scattering events cannot be seen as an electron changing its velocity along its path. Instead, the transport theory must be treated with many-body techniques, which in this work is handled by GF.

2.6.1 Green's functions

The GF has the interpretation that it transfers the effect of a source in a space-time point $(\boldsymbol{r}', t')$ to a point $(\boldsymbol{r}, t)$. In this subsection, the various GFs will be derived, and in section 3 they will finally be applied to transport theory in the NEGF approach.

Schrödinger equation

Consider the time-dependent Schrödinger equation

$$i\hbar\frac{\partial}{\partial t}\Psi(\boldsymbol{r}, t) - H\Psi(\boldsymbol{r}, t) = 0. \tag{2.63}$$

Suppose that there is a flash source in $\boldsymbol{r}$ at time t_i, then 2.63 becomes

$$i\hbar\frac{\partial}{\partial t}\Psi(\boldsymbol{r}, t) - H\Psi(\boldsymbol{r}, t) = s_i(\boldsymbol{r})\delta(t - t_i), \tag{2.64}$$

where $s_i(\boldsymbol{r})$ represents the source term. Integration over t gives the discontinuity equation for $\Psi(\boldsymbol{r}, t)$

$$i\hbar\big[\Psi(\boldsymbol{r}, t_{i+}) - \Psi(\boldsymbol{r}, t_{i-})\big] = s_i(\boldsymbol{r}), \tag{2.65}$$

and the solution for $t > t_i$ is given by (Jacoboni, 2010, p. 455)

$$\Psi(\boldsymbol{r}, t > t_i) = i\hbar \int g^r(\boldsymbol{r}, t, \boldsymbol{r}', t')\Psi(\boldsymbol{r}', t_i)\delta(t' - t_i)\mathrm{d}t'\mathrm{d}\boldsymbol{r}', \tag{2.66}$$

where $g^r(\boldsymbol{r}, t, \boldsymbol{r}', t')$ is the retarded GF and satisfies

$$\big(i\hbar\frac{\partial}{\partial t} - H\big)g^r(\boldsymbol{r}, t, \boldsymbol{r}', t') = \delta(\boldsymbol{r} - \boldsymbol{r}')\delta(t - t'). \tag{2.67}$$

After integrating 2.66 with respect to time, one obtains

$$\Psi(\boldsymbol{r}, t > t_i) = i\hbar \int g^r(\boldsymbol{r}, t, \boldsymbol{r}', t_i)\Psi(\boldsymbol{r}', t_i)\mathrm{d}\boldsymbol{r}'. \tag{2.68}$$

If one compares this with Equation 2.7, which has the solution

$$\Psi(\boldsymbol{r}, t) = \int U(\boldsymbol{r}, t, \boldsymbol{r}', t_0)\Psi(\boldsymbol{r}', t_0)\mathrm{d}\boldsymbol{r}', \tag{2.69}$$

it is obvious that the GF has the same interpretation as the time-evolution operator. The general relation between the two is

$$g^r(\boldsymbol{r}, t, \boldsymbol{r}', t') = \frac{1}{i\hbar}U(\boldsymbol{r}, t, \boldsymbol{r}', t')\theta(t - t'), \tag{2.70}$$

and

$$g^a(\boldsymbol{r}, t, \boldsymbol{r}', t') = -\frac{1}{i\hbar}U(\boldsymbol{r}, t, \boldsymbol{r}', t')\theta(t' - t) \tag{2.71}$$

for the advanced GF.

Second quantization Green's functions

In second quantization for a single particle state, the time-evolution operator can be written as

$$U(\boldsymbol{r}, t, \boldsymbol{r}', t') = \big\langle \boldsymbol{r}\big|U(t, t')\big|\boldsymbol{r}'\big\rangle. \tag{2.72}$$

The state $\big|\boldsymbol{r}\big\rangle$ can be obtained by applying the creation field to the vacuum state, so that $\big|\boldsymbol{r}\big\rangle = \Psi^\dagger(\boldsymbol{r})\big|0\big\rangle$. In the Heisenberg picture with time reference at t_0, the operator becomes

$$\begin{aligned}&\big\langle 0\big|\Psi(\boldsymbol{r})U(t, t')\Psi^\dagger(\boldsymbol{r}')\big|0\big\rangle = \\ &\big\langle 0\big|U(t, t_0)\Psi(\boldsymbol{r}, t)U^\dagger(t, t_0)U(t, t')U(t', t_0)\Psi^\dagger(\boldsymbol{r}', t')U^\dagger(t', t_0)\big|0\big\rangle,\end{aligned} \tag{2.73}$$

where it was used that $U(t', t_0)U^\dagger(t', t_0) = 1$. The three time evolution operators in the middle of 2.73 become 1, and the other two yield the unit

step function. Thus, for a single particle in the vacuum state, the GFs can be written as

$$g^r(\boldsymbol{r},t,\boldsymbol{r}',t') = \frac{1}{i\hbar}\big\langle 0\big|\Psi(\boldsymbol{r},t)\Psi^\dagger(\boldsymbol{r}',t')\big|0\big\rangle\theta(t-t') \tag{2.74}$$

$$g^a(\boldsymbol{r},t,\boldsymbol{r}',t') = -\frac{1}{i\hbar}\big\langle 0\big|\Psi(\boldsymbol{r},t)\Psi^\dagger(\boldsymbol{r}',t')\big|0\big\rangle\theta(t'-t) \tag{2.75}$$

Similarily, one may look at an arbitrary state by exchanging the vacuum state with a wavefunction, Φ in the following way

$$\big\langle\Phi_H\big|\Psi^\dagger(\boldsymbol{r},t)\Psi(\boldsymbol{r}',t')\big|\Phi_H\big\rangle, \tag{2.76}$$

where the subscript H denotes the Heisenberg picture.

The relation between the Heisenberg and the Schrödinger state is given by

$$\big|\Phi_H\big\rangle = U^{-1}(t,t_0)\big|\Phi_S(t)\big\rangle = U^{-1}(t,t_0)\int\big|\boldsymbol{r}\big\rangle\mathrm{d}\boldsymbol{r}\big\langle\boldsymbol{r}\big|\Phi_S(t)\big\rangle, \tag{2.77}$$

by using the completeness of the states $\big|\boldsymbol{r}\big\rangle$. The time evolution of the vacuum state will still be the vacuum state, so

$$U(t,t_0)\big|0\big\rangle = \big|0\big\rangle. \tag{2.78}$$

From this equation, the state becomes

$$\big|\Phi_H\big\rangle = \int\mathrm{d}\boldsymbol{r}\Phi_S(\boldsymbol{r},t)\Psi^\dagger(\boldsymbol{r},t)\big|0\big\rangle. \tag{2.79}$$

Equation 2.76 can now be written as

$$\int\mathrm{d}\boldsymbol{\rho}'\Phi_S^*(\boldsymbol{\rho}',t') \times\int\mathrm{d}\boldsymbol{\rho}\Phi_S(\boldsymbol{\rho},t)\big\langle 0\big|\Psi(\boldsymbol{\rho}',t')\Psi^\dagger(\boldsymbol{r}',t')\Psi(\boldsymbol{r},t)\Psi^\dagger(\boldsymbol{\rho},t)\big|0\big\rangle. \tag{2.80}$$

By using the relations in 2.29, and the fact that the annihilation operators give 0 when applied to the vacuum state, 2.80 can be written as

$$\begin{aligned}\big\langle\Phi_H\big|\Psi^\dagger(\boldsymbol{r},t)\Psi(\boldsymbol{r}',t')\big|\Phi_H\big\rangle &= \int \mathrm{d}\boldsymbol{\rho}'\Phi_S^*(\boldsymbol{\rho}',t') \\ &\times \int \mathrm{d}\boldsymbol{\rho}\Phi_S(\boldsymbol{\rho},t)\big\langle 0\big|\delta(\boldsymbol{r}'-\boldsymbol{\rho}')\delta(\boldsymbol{r}-\boldsymbol{\rho})\big|0\big\rangle.\end{aligned} \tag{2.81}$$

Integration over $\boldsymbol{\rho}$ and $\boldsymbol{r}$ yields

$$\big\langle\Phi_H\big|\Psi^\dagger(\boldsymbol{r},t)\Psi(\boldsymbol{r}',t')\big|\Phi_H\big\rangle = \Phi_S(\boldsymbol{r},t)\Phi_S^*(\boldsymbol{r}',t'). \tag{2.82}$$

The resulting Equation 2.82 shows that when $t \to t'$ and $\boldsymbol{r}' \to \boldsymbol{r}$, the field operators acting on the state gives the probability density $n(\boldsymbol{r}) = \big|\Phi(\boldsymbol{r},t)\big|^2$. So instead of obtaining a propagator one can define the GFs by, one rather obtains information about the system. If instead the reverse product $\Psi(\boldsymbol{r})\Psi^\dagger(\boldsymbol{r}')$ is applied to the Φ_H states, the result will be

$$\big\langle\Phi_H\big|\Psi(\boldsymbol{r},t)\Psi^\dagger(\boldsymbol{r}',t')\big|\Phi_H\big\rangle = \delta(\boldsymbol{r}-\boldsymbol{r}') \pm n(\boldsymbol{r}), \tag{2.83}$$

in the limits $\boldsymbol{r'} \to \boldsymbol{r}$ and $t' \to t$. With this in mind, the GFs can instead be defined as

$$G^r(\boldsymbol{r},t,\boldsymbol{r}',t') = \frac{1}{i\hbar}\big\langle\Phi_H\big|\big[\Psi(\boldsymbol{r},t),\Psi^\dagger(\boldsymbol{r}',t')\big]_\mp\big|\Phi_H\big\rangle\theta(t-t') \tag{2.84}$$

$$G^a(\boldsymbol{r},t,\boldsymbol{r}',t') = -\frac{1}{i\hbar}\big\langle\Phi_H\big|\big[\Psi(\boldsymbol{r},t),\Psi^\dagger(\boldsymbol{r}',t')\big]_\mp\big|\Phi_H\big\rangle\theta(t'-t) \tag{2.85}$$

Capital letters are used for these GFs as they are the central ones which will be used in the application to quantum cascade lasers.

For many-particle systems, the state $\big|\Phi_H\big\rangle$ must be replaced by an average over the entire ensebmle. The advanced GF is simply the complex conjugate of the retarded. Additionally, two other GFs are defined

$$G^n(\boldsymbol{r},t,\boldsymbol{r}',t') = \frac{1}{i\hbar}\big\langle\Psi(\boldsymbol{r},t)\Psi^\dagger(\boldsymbol{r}',t')\big\rangle \tag{2.86}$$

$$G^p(\boldsymbol{r},t,\boldsymbol{r}',t') = \pm\frac{1}{i\hbar}\big\langle\Psi(\boldsymbol{r}',t')\Psi^\dagger(\boldsymbol{r},t)\big\rangle \tag{2.87}$$

where G^n is called the electron GF, and G^p the hole correlation GF. Given these expressions, it is easy to realize that from the discussion above the

interpretation of these GFs is that they are correlation functions. G^n gives the correlation of the amplitude between a particle in $(\boldsymbol{r}, t)$ and $(\boldsymbol{r}', t')$, and $-G^p$ gives the correlation of available states to generate particles in $(\boldsymbol{r}', t')$ and $(\boldsymbol{r}, t)$.

Other GFs that will be used are the time ordered GFs, defined in the following way

$$\begin{aligned} G^t(\boldsymbol{r}, t, \boldsymbol{r}', t') &= \frac{1}{i\hbar}\big\langle T\Psi(\boldsymbol{r}, t)\Psi^\dagger(\boldsymbol{r}', t')\big\rangle \\ &= \theta(t - t')G^n + \theta(t' - t)G^p, \end{aligned} \tag{2.88}$$

and the anti-time ordered GF

$$G^{\bar{t}}(\boldsymbol{r}, t, \boldsymbol{r}', t') = \theta(t' - t)G^n + \theta(t - t')G^p. \tag{2.89}$$

From the definitions given for the various GFs, the following relations immediately follow

$$G^r = G^t - G^n = G^p - G^{\bar{t}} \tag{2.90}$$

$$G^a = G^t - G^n = G^p - G^{\bar{t}}. \tag{2.91}$$

2.6.2 Perturbation expansion of Green's functions

For a system with an interaction, the GFs may be expressed in terms of Feynman diagrams. In this work, the interaction picture is chosen because it is assumed that at a point in time or space perturbation is present.

Interaction picture

Using 2.11, and time evolving the Schrödinger state one obtains

$$\begin{aligned} \big|\Phi(t)\big\rangle_I = U_0^\dagger(t, t_0)\big|\Phi(t)\big\rangle_S = U_0^\dagger(t, t_0)U(t, t')\big|\Phi(t')\big\rangle_S = \\ U_0^\dagger(t, t_0)U(t, t')U_0(t', t_0)\big|\Phi(t')\big\rangle_I, \end{aligned} \tag{2.92}$$

keeping in mind that the subscript 0 denotes the use of the unperturbed Hamiltonian H_0. The operator, $U(t, t')$ evolves the Schrödinger state for

the full Hamiltonian, H. Thus, the time evolution operator in the interaction picture is

$$U_I(t,t') = U_0^\dagger(t,t_0)U(t,t')U_0(t',t_0) \tag{2.93}$$

Taking the time derivative gives the equation of motion for the time operator

$$\begin{aligned} i\hbar\frac{\mathrm{d}}{\mathrm{d}t}U_I(t,t') = &\Big(i\hbar\frac{\mathrm{d}}{\mathrm{d}t}U_0^\dagger(t,t_0)\Big)U(t,t')U_0(t',t_0) \\ &+U_0^\dagger(t,t_0)\Big(i\hbar\frac{d}{dt}U(t,t')\Big)U_0(t,t_0), \end{aligned} \tag{2.94}$$

where the last term is zero because $U_0(t',t_0)$ is independent of t. Furthermore, this becomes

$$i\hbar\frac{\mathrm{d}}{\mathrm{d}t}U_I(t,t') = U_0^\dagger(t,t_0)(-H_0+H)U(t,t')U_0(t',t_0). \tag{2.95}$$

Since $H = H_0 + H'$ the final expression is

$$i\hbar\frac{\mathrm{d}}{\mathrm{d}t}U_I(t,t') = H_I'U_I(t,t'), \tag{2.96}$$

with $H_I'(t) \equiv U_0^\dagger(t,t_0)H'U_0(t',t_0)$. Integration with respect to time t gives

$$U_I(t,t') = 1 + \frac{1}{i\hbar}\int_{t'}^{t} H_I'(t'')U_I(t'',t')\mathrm{d}t''. \tag{2.97}$$

Since H_I' is time-dependent, it is rarely the case that this equation may be solved exactly. Usually, for small perturbations one may instead substitute $U_I(t,t')$ into itself through 2.97 up to the desired order. To second order, the operator becomes

$$\begin{aligned} U_I(t,t') = 1 &+ \frac{1}{i\hbar}\int_{t'}^{t} H_I'(t'')\mathrm{d}t'' \\ &+ \frac{1}{(i\hbar)^2}\int_{t'}^{t}\int_{t'}^{t''} H_I'(t'')H_I'(t''')U_I(t''',t')\mathrm{d}t''\mathrm{d}t'''. \end{aligned} \tag{2.98}$$

Since this process can be repeated infinitely many times, the resulting expression on the right hand side will be an exponential function. With this,

and by ensuring correct time order of the operators, 2.97 can be expressed as

$$U_I(t,t') = T\exp\left(\frac{1}{i\hbar}\int_{t'}^{t} H_I'(\tau)\mathrm{d}\tau\right), \tag{2.99}$$

where T is the time ordering operator.

Feynman diagrams

In 2.86 and 2.87 the GFs were defined in the Heisenberg picture. Moving to the Schrödinger picture and looking at the electron correlation GF for a state $\Phi_S(t)$, it can be defined as

$$G^n(\boldsymbol{r},t,\boldsymbol{r}',t') = \frac{1}{i\hbar}\big\langle\Phi_S(t)\big|\Psi(\boldsymbol{r})U(t,t')\Psi^\dagger(\boldsymbol{r}')\big|\Phi_S(t')\big\rangle. \tag{2.100}$$

Using now 2.11 and 2.93, the greater GF in the interaction picture is

$$G^n(\boldsymbol{r},t,\boldsymbol{r}',t') = \frac{1}{i\hbar}\big\langle\Phi_I(t)\big|\Psi_I(\boldsymbol{r},t)U_I(t,t')\Psi_I^\dagger(\boldsymbol{r}',t')\big|\Phi_I(t')\big\rangle. \tag{2.101}$$

Time evolve now the states from time t_0

$$\begin{aligned} &G^n(\boldsymbol{r},t,\boldsymbol{r}',t') \\ &\quad= \frac{1}{i\hbar}\big\langle\Phi_I(t_0)\big|U_I^\dagger(t,t_0)\Psi_I(\boldsymbol{r},t)U_I(t,t')\Psi_I^\dagger(\boldsymbol{r}',t')U_I(t',t_0)\big|\Phi_I(t_0)\big\rangle, \end{aligned} \tag{2.102}$$

and insert the solution given by 2.99 gives

$$\begin{aligned} G^n(\boldsymbol{r},t,\boldsymbol{r}',t') = \frac{1}{i\hbar}\big\langle\Phi_I(t_0)\big|T\exp\left(\frac{1}{i\hbar}\int_{t}^{t_0} H_I'(\tau)\mathrm{d}\tau\right)\Psi_I(\boldsymbol{r},t) \\ \times T\exp\left(\frac{1}{i\hbar}\int_{t'}^{t} H_I'(\tau)\mathrm{d}\tau\right)\Psi_I^\dagger(\boldsymbol{r}',t') \\ \times T\exp\left(\frac{1}{i\hbar}\int_{t_0}^{t'} H_I'(\tau)\mathrm{d}\tau\right)\big|\Phi_I(t_0)\big\rangle. \end{aligned} \tag{2.103}$$

It is now convenient to introduce the contour time ordering operator, T_c, to simplify the above expression

$$G^n(\boldsymbol{r},t,\boldsymbol{r}',t') = \frac{1}{i\hbar}\left\langle T_c\Big\{ \exp\left(\frac{1}{i\hbar}\int_C H_I'(\tau)\mathrm{d}\tau\right)\Psi_I(\boldsymbol{r},t)\Psi_I^\dagger(\boldsymbol{r}',t')\Big\}\right\rangle \quad (2.104)$$

The contour ordering operator is defined such that the times in the contour from t_0 back to itself must be kept in the correct order. See Figure 2.2 for details.

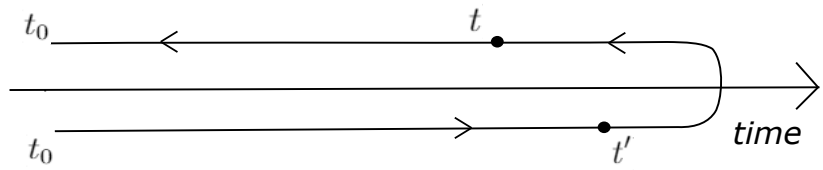

Figure 2.2: Contour integration for the case where $t > t'$ on the forward path, but t is closer to t_0 on the path back on the contour, C.

Without prescription of the location of the two times t and t' in 2.104, it becomes the general GF here denoted G. Expanding the exponential factor to order zero, it will simply be 1 so that the unperturbed GF becomes

$$G_0(\boldsymbol{r},t,\boldsymbol{r}',t') = \frac{1}{i\hbar}\Big\langle T_c\Big\{\Psi_I(\boldsymbol{r},t)\Psi_I^\dagger(\boldsymbol{r}',t')\Big\}\Big\rangle. \quad (2.105)$$

The corresponding Feynman diagram is drawn in Figure 2.3.
The first order term is linear in the potential, so

$$G_1(\boldsymbol{r},t,\boldsymbol{r}',t') = \frac{1}{i\hbar}\left\langle T_c\left\{\frac{1}{i\hbar}\int H_I'(\tau)\mathrm{d}\tau\Psi_I(\boldsymbol{r},t)\Psi_I^\dagger(\boldsymbol{r}',t')\right\}\right\rangle. \quad (2.106)$$

For a simple potential, $V(\boldsymbol{r})$ the interaction Hamiltonian in second quantization can be written as $H_I'(t) = \int \Psi_I^\dagger(\boldsymbol{r},t)V(\boldsymbol{r})\Psi_I(\boldsymbol{r},t)$. Inserting this into 2.106 gives

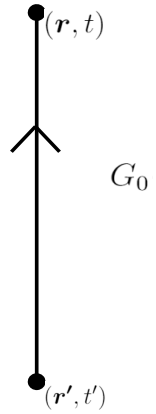

Figure 2.3: The zeroth order term, G_0, simply propagates a particle in point $(\boldsymbol{r}', t')$ to $(\boldsymbol{r}, t)$.

$$G_1(\boldsymbol{r}, t, \boldsymbol{r}', t') = \frac{1}{(i\hbar)^2} \times \left\langle T_c \Big\{ \int \int \mathrm{d}\boldsymbol{r}'' \Psi_I^\dagger(\boldsymbol{r}'', \tau) V(\boldsymbol{r}'') \Psi_I(\boldsymbol{r}'', \tau) \Psi_I(\boldsymbol{r}, t) \Psi_I^\dagger(\boldsymbol{r}', t') \Big\} \right\rangle. \tag{2.107}$$

By using the Wick-Matsubara theorem from subsection 2.4.3, the operators can be split into three terms

$$\begin{aligned} V(\boldsymbol{r}'') \Big\{ & \big\langle T_c\big\{ \Psi_I^\dagger(\boldsymbol{r}'', \tau) \Psi_I(\boldsymbol{r}, t) \big\} \big\rangle \big\langle T_c\big\{ \Psi_I(\boldsymbol{r}'', \tau) \Psi_I^\dagger(\boldsymbol{r}', t') \big\} \big\rangle \\ & \pm \big\langle T_c\big\{ \Psi_I^\dagger(\boldsymbol{r}'', \tau) \Psi_I(\boldsymbol{r}'', \tau) \big\} \big\rangle \big\langle T_c\big\{ \Psi_I(\boldsymbol{r}, t) \Psi_I^\dagger(\boldsymbol{r}', t') \big\} \big\rangle \\ & + \big\langle T_c\big\{ \Psi_I^\dagger(\boldsymbol{r}'', \tau) \Psi_I^\dagger(\boldsymbol{r}', t') \big\} \big\rangle \big\langle T_c\big\{ \Psi_I(\boldsymbol{r}'', \tau) \Psi_I(\boldsymbol{r}, t) \big\} \big\rangle \Big\}, \end{aligned} \tag{2.108}$$

where the factor $1/(i\hbar)^2$ was neglected for readability. The last term is zero, as there are two creation and annihilation operators acting on the state. Thus, 2.108 can be expressed as

$$\begin{aligned} V(\boldsymbol{r}'') \Big\{ & G_0(\boldsymbol{r}'', \tau, \boldsymbol{r}, t) G_0(\boldsymbol{r}'', \tau, \boldsymbol{r}', t') \\ & \pm G_0(\boldsymbol{r}'', \tau, \boldsymbol{r}'', \tau) G_0(\boldsymbol{r}, t, \boldsymbol{r}', t') \Big\} \end{aligned} \tag{2.109}$$

The two resulting Feynman diagrams are shown in Figure 2.4. This process of substituting the interaction potential may be repeated for all orders, but the complexity drastically increases. Already for second order, there are six terms similar to those in 2.109.

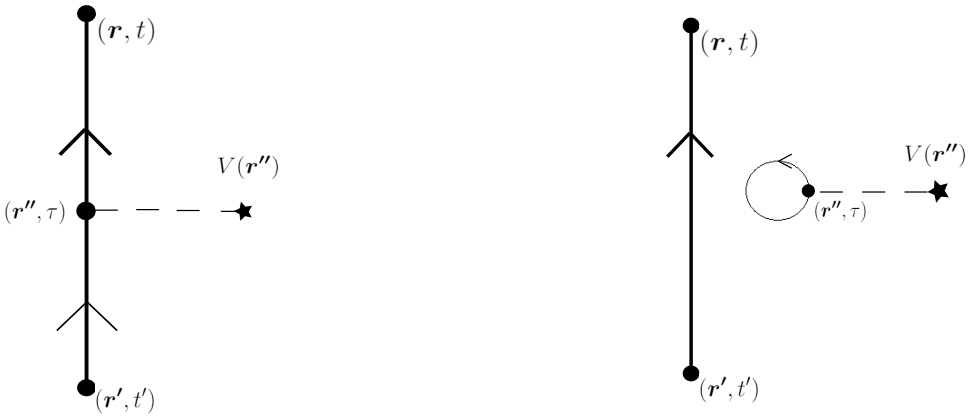

Figure 2.4: Diagrams of the first order Green function, $G^{(1)}$. The star denotes the space-time point of the potential interaction. The diagram to the left is fully connected, while the diagram to the right is disconnected.

Dyson equation and self-energy

Continuing the expansion of the GF, for each order new disconnected diagrams will be obtained. However, all of the disconnected diagrams will vanish. This is because in the expression for those diagrams, the GF simply describes a propagation from a point back to itself. This is a loop which becomes zero, so for instance in 2.109 the last term will disappear. Similar results happen for higher orders. Thus, since only the connected parts are left, the GF expansion may be written as

$$\begin{aligned} G &= G_0 + G_0 V G_0 + G_0 V G_0 V G_0 + ... \\ &= G_0 + G_0 V \big[G_0 + G_0 V G_0 + ... \big]. \end{aligned} \tag{2.110}$$

The term in the brackets is simply the GF itself. Because the GF is equal to itself, the potential V is called the self-energy and is substituted by the letter Σ. Collecting $G_0 \Sigma$ to the left or ΣG_0 to the right results in the two forms of the Dyson equation

$$G = G_0 + G_0 \Sigma G, \quad G = G_0 + G \Sigma G_0. \tag{2.111}$$

Solving this gives

$$G = \frac{1}{G_0^{-1} - \Sigma}, \tag{2.112}$$

which gives the interpretation that Σ acts as a correction to the unperturbed GF because of the interactions considered. This equation holds for all the different types of GFs. For the retarded GF, 2.112 becomes

$$G^r = \frac{1}{(G_0^r)^{-1} - \Sigma^r}, \tag{2.113}$$

note that the self-energy is different in the retarded and advanced case. Recall from subsection 2.6.1, the retarded GF at equilibrium is the inverse of the Schrödinger equation. Thus, the equation for the retarded GF becomes

$$G^r = \frac{1}{i\hbar\partial/\partial t - H_0 - \Sigma^r}, \tag{2.114}$$

and the advanced is simply the complex conjugate, $G^a = (G^r)^*$. When applied to the states of the system, the operator $i\hbar\partial/\partial t$ will simply yield the eigenenergy, E.

Lastly, the Dyson equation for the lesser and greater GFs will be found. By using that $\Sigma^r = \Sigma^t - \Sigma^< = \Sigma^{\bar{t}} - \Sigma^>$, $\Sigma^a = \Sigma^t - \Sigma^> = \Sigma^< - \Sigma^{\bar{t}}$, 2.90 and 2.91, one may obtain the following

$$G^n = G_0^n + G_0^n \Sigma^t G^t - G_0^{\bar{t}} \Sigma^{in} G^t - G_0^n \Sigma^{out} G^n + G_0^{\bar{t}} \Sigma^{\bar{t}} G^n, \tag{2.115}$$

$$G^p = G_0^p + G_0^p \Sigma^{\bar{t}} G^{\bar{t}} - G_0^t \Sigma^p G^{\bar{t}} - G_0^p \Sigma^{in} G^p + G_0^t \Sigma^t G^p. \tag{2.116}$$

Using now that $G^t = G^r + G^p$, $G^{\bar{t}} = G^p - G^a$, $\Sigma^t = \Sigma^r + \Sigma^{out}$, $\Sigma^{\bar{t}} = \Sigma^{out} - \Sigma^a$ and $\Sigma^{in} = \Sigma^r + \Sigma^r = \Sigma^r + \Sigma^{out} - \Sigma^a$ from the definitions at the end of subsection 2.6.1 one may obtain

$$\left(1 - G_0^r \Sigma^r\right) G^p = G_0^p (1 + \Sigma^a G^a) + G_0^r \Sigma^{out} G^a. \tag{2.117}$$

Using 2.111 for the retarded GF, and multiplying with $\left(1 + G^r \Sigma^r\right)$ gives

$$G^p = \big(1 + G^r \Sigma^r\big) G_0^p \big(1 + \Sigma^a G^a\big) + G^r \Sigma^{out} G^a \tag{2.118}$$
$$G^n = \big(1 + G^r \Sigma^r\big) G_0^n \big(1 + \Sigma^a G^a\big) + G^r \Sigma^{in} G^a. \tag{2.119}$$

It is now useful to move to the momentum representation of the GFs. The Dyson equation for the retarded and advanced GFs now become

$$G^{r/a}(\boldsymbol{k}, \omega) = G_0^{r/a} + (2\pi)^3 G_0^{r/a}(\boldsymbol{k}, \omega) \Sigma^{r/a}(\boldsymbol{k}, \omega) G^{r/a}(\boldsymbol{k}, \omega), \tag{2.120}$$

with the solution

$$G^{r/a}(\boldsymbol{k}, \omega) = \frac{1}{(2\pi)^{3/2}\hbar} \frac{1}{\omega - \omega_{\boldsymbol{k}} - (2\pi)^{3/2} \Sigma^{r/a}/\hbar}. \tag{2.121}$$

Since the self-energy is in general complex, it may be defined in the following way

$$\Sigma^r(\boldsymbol{k}, \omega) = \frac{\hbar}{(2\pi)^{3/2}} \big(\omega_s - i\Gamma\big), \tag{2.122}$$

where ω_s is a shift in the energy eigenvalues, Γ is the lifetime of the eigenstates and $\Sigma^a = \big(\Sigma^r\big)^*$. From 2.120, the retarded GF becomes

$$G^r(\boldsymbol{k}, \omega) = \frac{1}{(2\pi)^{3/2}\hbar} \frac{1}{\sigma + i\Gamma}, \tag{2.123}$$

where $\sigma = \omega - \omega_{\boldsymbol{k}} - \omega_s$. The new equation for the hole GF is now

$$G^p = \big(1 + (2\pi)^3 G^r \Sigma^r\big) G_0^p \big(1 + (2\pi)^3 \Sigma^a G^a\big) + (2\pi)^3 G^r \Sigma^{out} G^a. \tag{2.124}$$

G_0^p is proportional to $\delta(\omega - \omega_{\boldsymbol{k}})(\omega - \omega_{\boldsymbol{k}})^2$ which is zero. So one is left with

$$G^p = (2\pi)^3 G^r \Sigma^{out} G^a \tag{2.125}$$
$$G^n = (2\pi)^3 G^r \Sigma^{in} G^a, \tag{2.126}$$

again with very similar derivations for G^n.

2.7 Finite difference scheme

One way to solve both the SP and the NEGF equations numerically, is to discretize them into finite steps with uniform spacing. More specifically, they are solved using FDM.

The Hamiltonian which enter either SP or NEGF is on the form

$$H = -\frac{\hbar^2}{2m}\frac{\partial^2}{\partial z^2} + U(z), \tag{2.127}$$

for some single particle potential $U(z)$. Using FDM, all derivatives of complex functions are expressed as

$$\frac{\partial f}{\partial x} \approx \frac{1}{d}\big[f_i - f_j\big] \tag{2.128}$$

$$\frac{\partial^2 f}{\partial x^2} \approx \frac{1}{d^2}\big[f_i - 2f_j + f_k\big]. \tag{2.129}$$

The indices, i, j, k denote three neighbouring points on the grid, and d is the spacing between the points. Equations 2.128 and 2.129 are used in order to find the derivatives of the states of the system.

The resulting discretized Hamiltonian will be of the tridiagonal form

$$H_{ij} = \begin{bmatrix} U_1 + 2t & -t & 0 & \dots & 0 \\ -t & U_2 + 2t & 0 & \dots & 0 \\ 0 & -t & U_3 + 2t & \dots & 0 \\ \dots & & & & \end{bmatrix}, \tag{2.130}$$

where $t = \hbar^2/2md^2$. This will be explained in more detail in section 3.1.

Chapter 3

Numerical model

3.1 Recursive solutions

This section will explain how the SP and NEGF equations may be solved numerically, and implemented using a programming language.

3.1.1 Schrödinger-Poisson solver

Schrödinger equation

Using the FDM as described in 2.7 on a spatial grid with uniform spacing Δ_z, 2.55 can be discretely solved. The first order derivative is approximated as $\partial_z\psi(z_n+1/2) \approx \Delta\psi_{n+1/2}$. Using linear interpolation (Jirauschek, 2009, p. 1062), this becomes

$$\Delta\psi_{n+1/2} = \big(\psi_{n+1} - \psi_n\big)/\Delta_z. \tag{3.1}$$

The term involving the effective mass in 2.55 can then be expressed as

$$\partial_z\big(m^*(z)\big)^{-1}\partial_z\psi(z) = (\Delta\psi_{n+1/2}/m^*_{n+1/2} - \Delta\psi_{n-1/2}/m^*_{n-1/2})/\Delta_z. \tag{3.2}$$

Using the same technique as above, the effective mass becomes

$$m^*_{n+1/2} = (m^*_n + m^*_{n+1})/2. \tag{3.3}$$

Finally, 2.55 is discretized into

$$-s_n\psi_{n-1} + d_n\psi_n - s_{n+1}\psi_{n+1} = E\psi_n, \tag{3.4}$$

where

$$s_n \equiv \frac{\hbar^2}{\Delta_z^2(m^*_{n-1} + m^*_n)} \tag{3.5}$$

and

$$d_n \equiv \frac{\hbar^2}{\Delta_z^2}\left(\frac{1}{m^*_{n-1} + m^*_n} + \frac{1}{m^*_n + m^*_{n+1}}\right) + V_n. \tag{3.6}$$

Equation 3.4 can now be transformed into a matrix equation, and solved assuming the boundary conditions $\psi_0 = 0 = \psi_N$. Here, N is the final grid point. This gives the matrix equation

$$\Big(\boldsymbol{H} - E\boldsymbol{I}\Big)\boldsymbol{\psi} = 0, \tag{3.7}$$

where $\boldsymbol{\psi} = \big\{\psi_1, \psi_2, ..., \psi_N\big\}^T$, $\boldsymbol{I}$ is the identity matrix of dimension $N-1$, and $\boldsymbol{H}$ contains the following elements

$$H_{n,n} = d_n \tag{3.8}$$

$$H_{n,n-1} = -s_n \tag{3.9}$$

$$H_{n,n+1} = -s_{n+1} \tag{3.10}$$

where all other elements are zero. Thus, 3.7 can be solved as a tridiagonal eigenvalue problem.

Poisson equation

By using the same approach for the Poisson as for the Schrödinger equation, the resulting discretized form of 2.56 becomes

$$\tilde{s}_n\widetilde{V}_n - \tilde{d}_n\widetilde{V}_n + \tilde{s}_{n+1}\widetilde{V}_{n+1} = \rho_n, \tag{3.11}$$

where now

$$\tilde{s}_n \equiv \frac{1}{2e\Delta_z^2}\Big(\epsilon_{n-1} + \epsilon_n\Big), \tag{3.12}$$

$$\tilde{d}_n \equiv \frac{1}{2e\Delta_z^2}\Big(\epsilon_{n-1} + 2\epsilon_n + \epsilon_{n+1}\Big), \tag{3.13}$$

and

$$\rho_n \equiv e\left(N_{D,n} + \sum_i n_{i,n}\big|\psi_{i,n}\big|^2\right). \tag{3.14}$$

Thus, the length of the grid that 3.11 is solved for must coincide with the length of the grid used to solve 3.4. Using similar boundary conditions $\widetilde{V}_0 = 0 = \widetilde{V}_N$, the following matrix equation is obtained

$$\boldsymbol{M}\widetilde{\boldsymbol{V}} = \boldsymbol{\rho}, \tag{3.15}$$

with

$$\widetilde{\boldsymbol{V}} = \big\{\widetilde{V}_1, \widetilde{V}_2, ..., \widetilde{V}_N\big\} \tag{3.16}$$

$$\boldsymbol{\rho} = \big\{\rho_1, \rho_2, ..., \rho_N\big\}. \tag{3.17}$$

The matrix $\boldsymbol{M}$ has the only non-zero elements

$$M_{n,n} = -\tilde{d}_n \tag{3.18}$$

$$M_{n,n-1} = \tilde{s}_n \tag{3.19}$$

$$M_{n,n+1} = \tilde{s}_{n+1}. \tag{3.20}$$

So 3.11 is also solved as a tridiagonal eigenvalue problem.

3.1.2 Nonequilibrium Green's function solver

The following subsection describes exactly how the NEGF equations may be iteratively solved. The biggest problem when solving 2.114 is that even though $(E - H_0 - \Sigma^r)$ is a sparse matrix, the GFs will be full matrices. This means that a tremendous amount of processing power and storage is required to calculate these matrices. However, instead of calculating all elements, only the diagonal "blocks" need to be calculated. Then, one may decide which off-diagonal terms need to be calculated after this.

Hamiltonian and basis

The following Hamiltonian describes the system in this work

$$H = H_0 + H_{pop} + H_{ac} + H_{ir} + H_{al} + H_{id}, \tag{3.21}$$

where the subscripts respectively mean polar optical phonons, acoustic phonons, interface roughness, alloy disorders, and ionized dopants or impurities. The perturbative terms can be included in a self-energy, Σ. The unperturbed Hamiltonian is broken down into the following parts

$$H_0 = H_0^D + H_0^L + H_0^R + H_0^{LD} + H_0^{RD}, \tag{3.22}$$

where each term respectively represents the Hamiltonian of the device, the left and right contacts, the coupling between the left contact and the device and the coupling between the right contact and the device. Note that since the unperturbed Hamiltonian by definition is known, its solution will be exact.

For the compound GaAs, the element Ga is the cation and As the anion. For alternating layers of cations and anions, a vector which points to a layer L of the cations has a z-component of $\boldsymbol{R}_z^L = L\Delta$ and an in-plane component $\boldsymbol{R}_t^L$. Here, Δ is the spacing of each layer. Likewise, the anions have the same components except that they are shifted by a vector $\boldsymbol{v} = \frac{\Delta}{2}(1,1,1)$ from each cation layer. The basis for the cations and anions respectively are $\big|c, L, \boldsymbol{R}_t^L\big\rangle$ and $\big|a, L, \boldsymbol{R}_t^L\big\rangle$. Both a and c run over all possible orbitals. The bases are then given by the Bloch states

$$\big|c, L, \boldsymbol{k}\big\rangle = \frac{1}{\sqrt{N}} \sum_{\boldsymbol{R}_t^L} \exp(i\boldsymbol{k} \cdot \boldsymbol{R}_t^L) \big|c, L, \boldsymbol{R}_t^L\big\rangle \tag{3.23}$$

$$\big|a, L, \boldsymbol{k}\big\rangle = \frac{1}{\sqrt{N}} \sum_{\boldsymbol{R}_t^L} \exp(i\boldsymbol{k} \cdot (\boldsymbol{R}_t^L + \boldsymbol{v})) \big|a, L, \boldsymbol{R}_t^L\big\rangle, \tag{3.24}$$

for some normalization factor N. The field operators then become

$$\Psi(\boldsymbol{r}) = \sum_{\boldsymbol{k}, L} \left[\sum_c \big\langle \boldsymbol{r} \big| c, L, \boldsymbol{k} \big\rangle c_{c,L,\boldsymbol{k}} + \sum_a \big\langle \boldsymbol{r} \big| a, L, \boldsymbol{k} \big\rangle c_{a,L,\boldsymbol{k}} \right], \tag{3.25}$$

where $c_{c,L,\boldsymbol{k}}$ and $c_{a,L,\boldsymbol{k}}$ respectively are the destruction operators for an electron in the state $\big|c, L, \boldsymbol{k}\big\rangle$ and $\big|a, L, \boldsymbol{k}\big\rangle$.

The matrix elements of the unperturbed Hamiltonian is in general

$$\begin{aligned}\big\langle \alpha, L, \boldsymbol{k}\big|H_0\big|\alpha', L', \boldsymbol{k}\big\rangle = D_{\alpha,\alpha';L'}(\boldsymbol{k})\delta_{L,L'} \\ -t_{\alpha,L;\alpha',L'}(\boldsymbol{k})\delta_{L',L\pm j\neq 0},\end{aligned} \tag{3.26}$$

where the index j is an integer. In the single-band and tight-binding approximations, this Hamiltonian becomes tri-diagonal with elements

$$t_{i,j} \equiv \frac{\hbar^2}{(m_i + m_j)\Delta^2} \tag{3.27}$$

$$D_i(k) \equiv \frac{\hbar^2}{2\Delta^2}\left(\frac{1}{m^-} + \frac{1}{m^+}\right)V_i \tag{3.28}$$

$$m^- \equiv \frac{m_{i-1} + m_i}{2} \tag{3.29}$$

$$m^+ \equiv \frac{m_i + m_{i+1}}{2}. \tag{3.30}$$

It is now clear that this unperturbed Hamiltonian corresponds with the Hamiltonian found in the subsection 3.1.1, which is a relief. The difference between the Hamiltonian for the entire system in the NEGF case and the one for the SP solver, is that the former includes the perturbative self-energy term.

The retarded Green's function

The Dyson equation is on the form $AG^r = I$ where I is the identity matrix needs to be solved. The solution becomes

$$(G^r)^{-1} = \begin{bmatrix} A_{0,0} & t_{0,1} & 0 & \dots & 0 \\ t_{1,0} & A_{1,1} & t_{1,2} & \dots & 0 \\ 0 & t_{2,1} & A_{3,3} & \dots & 0 \\ \dots & \dots & \dots & \dots & t_{N-2,N-1} \\ 0 & 0 & \dots & t_{N-1,N-2} & A_{N-1,N-1} \end{bmatrix}, \tag{3.31}$$

where $A_{i,i}$ is the Dyson equation for block number i.

Since none of the blocks are currently known, the Dyson equation can for instance be solved for two consecutive blocks (D. Vasileska and Klimeck, 2010, p. 526-533). The equation then becomes

$$\begin{bmatrix} A_{Z,Z} & A_{Z,Z'} \\ A_{Z',Z} & A_{Z',Z'} \end{bmatrix} \begin{bmatrix} G^r_{Z,Z} & G^r_{Z,Z'} \\ G^r_{Z',Z} & G^r_{Z',Z'} \end{bmatrix} = \begin{bmatrix} I & 0 \\ 0 & I \end{bmatrix}, \tag{3.32}$$

This has the solution

$$G^r = G^r_0 + G^r U G^r_0, \tag{3.33}$$

where

$$G^r_0 = \begin{bmatrix} (G^r_{Z,Z})_0 & 0 \\ 0 & (G^r_{Z',Z'})_0 \end{bmatrix} = \begin{bmatrix} A^{-1}_{Z,Z} & 0 \\ 0 & A^{-1}_{Z',Z'} \end{bmatrix} \tag{3.34}$$

and

$$U = \begin{bmatrix} 0 & -A^{-1}_{Z,Z'} \\ -A^{-1}_{Z',Z} & 0 \end{bmatrix}. \tag{3.35}$$

The equation for the advanced GF can be solved in the exact same way, except now G^a is the complex transpose of G^r, $G^a = (G^r)^*$.

In order to solve the system by GF techniques, it is necessary to assume that the contacts have semi-infinite domain. Otherwise, there would be an infinite amount of equations. Assume that the block indexed zero lies somewhere in the regime of the left contact, not too far away from the device as indicated in Figure 3.1. Then suppose that all of the blocks to the left of block indexed -2, which is an infinite amount of blocks are assumed to have the same values as the block in -2. Then the left connected GF is given by the matrix

$$(g^{Lr})^{-1}_{0,0} = \begin{bmatrix} E - A_{-2,-2} - \Sigma^r_{-2,-2} & A_{-2,-1} & 0 \\ A_{-1,-2} & E - A_{-1,-1} & A_{-1,0} \\ 0 & A_{0,-1} & E - A_{0,0} \end{bmatrix}. \tag{3.36}$$

Because the block is in the upper left corner, the superscript L is added. The same can be done for each block along the diagonal of the system. The recursive solutions

$$g^{Lr}_{i,i} = \left(A_{i,i} - A_{i,i-1} g^{Lr}_{i-1,i-1} A_{i-1,i}\right)^{-1} \tag{3.37}$$

for a diagonal block follow from 3.33 for the consecutive blocks $Z = i - 1$ and $Z' = i$. The last block, $g^{Lr}_{N-1,N-1}$ is special, because it contains information about the entire system between the contacts. And this is simply the retarded GF, $G^r_{N-1,N-1} = g^{Lr}_{N-1,N-1} = G^r$.

Since the last element of the retarded GF is known, this can be used to recursively find the other elements. The off-diagonal terms can be found by the equations

$$G^r_{i>j,j} = -g_{i,i} t_{i+1,i} G^r_{i,j+1} \tag{3.38}$$

$$G^r_{i,j>i} = -g_{i,i} t_{i,i+1} G^r_{i+1,j} \tag{3.39}$$

For the diagonal elements, the equation becomes

$$G^r_{i,i} = g^{Lr}_{i,i}(1 - A_{i,i+1} G^r_{i+1,i}). \tag{3.40}$$

Indexation is different from before, because now the algorithm starts on the last element of G^r and walks the other way to find the remaining diagonal elements.

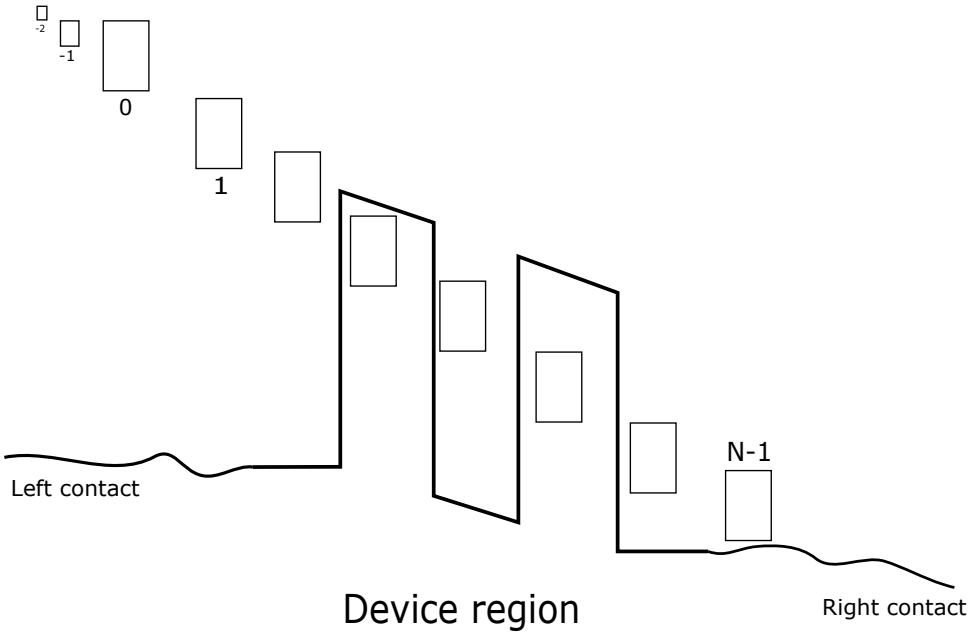

Figure 3.1: Blocks iterated throughout the system using FDM and the method described in the text. The sizes and numbers of blocks are only representative of the actual process, the blocks may be smaller and the number larger.

The entire ”walking” process is shown in Figure 3.2. If densities are needed for particular regions, this can be easily found by using 3.38 and 3.39. This technique demonstrates that it is not necessary to know all of the elements of the GFs in order to simulate the physical processes of the system. Only diagonal blocks need to be calculated, and then calculating the other desired GF blocks afterwards.

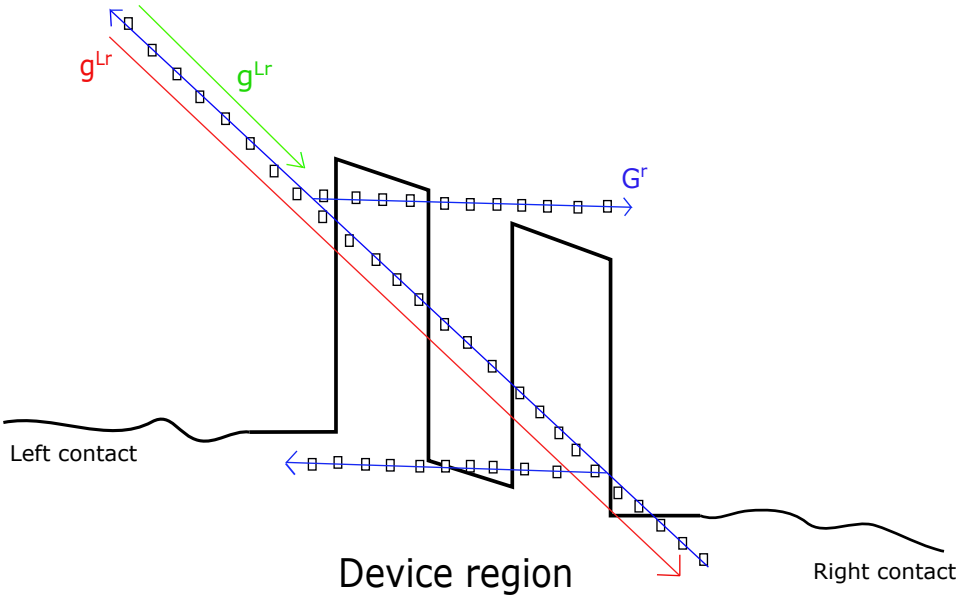

Figure 3.2: Green functions for the numerical process. In order to find G^r, one must ”walk” g^{Lr} through the entire system and connect it to G^r in the last block. Then, electron or current densities can be found by ”walking” back and finding the horizontal blocks indicated by the blue lines. If only the current on one side is needed, the only block that has to be calculated is the one to the left of the device indicated by the green line.

The correlation Green's function

Equations 2.125 and 2.126 are solved by using the same techniques as for the retarded and advanced GFs, which are on the form

$$AG^n = \Sigma^n G^a \tag{3.41}$$
$$AG^p = \Sigma^p G^a. \tag{3.42}$$

By following the previous conventions, the matrix form of this is

$$\begin{bmatrix} A_{Z,Z} & A_{Z,Z'} \\ A_{Z',Z} & A_{Z',Z'} \end{bmatrix} \begin{bmatrix} G^n_{Z,Z} & G^n_{Z,Z'} \\ G^n_{Z',Z} & G^n_{Z',Z'} \end{bmatrix} = \begin{bmatrix} \Sigma^n_{Z,Z} & \Sigma^n_{Z,Z'} \\ \Sigma^n_{Z',Z} & \Sigma^n_{Z',Z'} \end{bmatrix} \begin{bmatrix} G^a_{Z,Z} & G^a_{Z,Z'} \\ G^a_{Z',Z} & G^a_{Z',Z'} \end{bmatrix}, \quad (3.43)$$

taking into account the electron correlation GF. The hole correlation GF follows the exact same procedure. This yields the following solutions

$$G^n = G^r_0 U G^n + G^r_0 \Sigma^{in} G^a \quad (3.44)$$
$$G^p = G^r_0 U G^p + G^r_0 \Sigma^{out} G^a. \quad (3.45)$$

or

$$G^n = G^n_0 + G^r U G^n_0 + G^n U^\dagger G^a_0, \quad (3.46)$$

where $G^n_0 = G^r_0 \Sigma^{in} G^a_0$ and 3.33 was used.

The first block has the solution for each of the GFs

$$g^{Ln}_{0,0} = g^{Lr}_{0,0} \Sigma^{in}_{0,0} g^{La}_{0,0} \quad (3.47)$$
$$g^{Lp}_{0,0} = g^{Lr}_{0,0} \Sigma^{out}_{0,0} g^{La}_{0,0}, \quad (3.48)$$

and the other diagonal blocks are given by

$$g^{Ln}_{i,i} = g^{Lr}_{i,i} \big[\Sigma^{in}_{i,i} + A_{i,i-1} g^{Ln}_{i-1,i-1} A^\dagger_{i-1,i} - \Sigma^{in}_{i,i-1} g^{La}_{i-1,i-1} A^\dagger_{i-1,i} - A_{i,i-1} g^{Lr}_{i-1,i-1} \Sigma^{in}_{i-1,i} \big] g^{La}_{i,i}, \quad (3.49)$$

$$g^{Lp}_{i,i} = g^{Lr}_{i,i} \big[\Sigma^{out}_{i,i} + A_{i,i-1} g^{Lp}_{i-1,i-1} A^\dagger_{i-1,i} - \Sigma^{out}_{i,i-1} g^{La}_{i-1,i-1} A^\dagger_{i-1,i} - A_{i,i-1} g^{Lr}_{i-1,i-1} \Sigma^{out}_{i-1,i} \big] g^{La}_{i,i}. \quad (3.50)$$

The connected correlation GFs then become

$$G^n_{i,i} = g^{Ln}_{i,i} + g^{Lr}_{i,i} A_{i,i+1} G^n_{i+1.i+1} A^\dagger_{i+1,i} g^{La}_{i,i} - (g^{Ln}_{i,i} A^\dagger_{i,i+1} G^a_{i+1,i} + G^r_{i,i+1} A_{i+1,i} g^{Ln}_{i,i}) \quad (3.51)$$

$$G^p_{i,i} = g^{Lp}_{i,i} + g^{Lr}_{i,i} A_{i,i+1} G^p_{i+1.i+1} A^\dagger_{i+1,i} g^{La}_{i,i} - (g^{Lp}_{i,i} A^\dagger_{i,i+1} G^a_{i+1,i} + G^r_{i,i+1} A_{i+1,i} g^{Lp}_{i,i}). \quad (3.52)$$

The off-diagonal elements are

$$\begin{aligned} G^n_{i+1,i} &= (g^{Ln}_{i+1,i})_0 - G^r_{i+1,i}A_{i,i+1}(g^{Ln}_{i+1,i})_0 \\ &-G^r_{i+1,i+1}A_{i+1,i}g^{Ln}_{i,i} - G^{Ln}_{i+1,i+1}A^\dagger_{i+1,i}g^{La}_{i,i} \end{aligned} \tag{3.53}$$

$$\begin{aligned} G^p_{i+1,i} &= (g^{Lp}_{i+1,i})_0 - G^r_{i+1,i}A_{i,i+1}(g^{Lp}_{i+1,i})_0 \\ &-G^r_{i+1,i+1}A_{i+1,i}g^{Lp}_{i,i} - G^{Lp}_{i+1,i+1}A^\dagger_{i+1,i}g^{La}_{i,i}, \end{aligned} \tag{3.54}$$

and

$$\begin{aligned} G^n_{i,i+1} &= (g^{Ln}_{i,i+1})_0 - G^r_{i,i+1}A_{i+1,i}(g^{Ln}_{i,i+1})_0 \\ &-G^r_{i,i}A_{i,i+1}g^{Ln}_{i+1,i+1} - G^n_{i,i}A^\dagger_{i,i+1}g^{La}_{i+1,i+1} \end{aligned} \tag{3.55}$$

$$\begin{aligned} G^p_{i,i+1} &= (g^{Ln}_{i,i+1})_0 - G^r_{i,i+1}A_{i+1,i}(g^{Lp}_{i,i+1})_0 \\ &-G^r_{i,i}A_{i,i+1}g^{Lp}_{i+1,i+1} - G^p_{i,i}A^\dagger_{i,i+1}g^{La}_{i+1,i+1}. \end{aligned} \tag{3.56}$$

3.1.3 Expressions for the self-energies

For the moment, only the contact self-energies are considered such that the governing equations are

$$\left[E - H_0 - \Sigma^r_{lead}\right]G^r = 1 \tag{3.57}$$

where Σ^r_{lead} is the retarded self-energy for the leads, and

$$G^n = G^r\,\Sigma^{in}_{lead}G^a, \tag{3.58}$$

Due to the semi-infinite contacts, the self-energies are

$$(\Sigma^r_{lead})_{-2,-2} = A_{-2,-3}g^{Lr}_{-3,-3}A_{-3,-2}, \tag{3.59}$$

for the contact to the left and

$$(\Sigma^r_{lead})_{N-1,N-1} = A_{N-2,N-1}g^{Lr}_{N-1,N-1}A_{N-1,N-2} \tag{3.60}$$

for the right. The expressions for the advanced self-energies are exactly the same, except g^{Lr} is replaced by g^{La}. The self-energies related to the scattering into the device are given by

$$(\Sigma^{in}_{lead})_{0,0} = A_{1,0}g^{Ln}_{0,0}A_{0,1} \tag{3.61}$$

at the left boundary and

$$(\Sigma^{in}_{lead})_{N-1,N-1} = A_{N-2,N-1} g^{Ln}_{N-1,N-1} A_{N-1,N-2} \tag{3.62}$$

at the right boundary.

Since the solution of $g^{Lr}_{-3,-3}$ is needed to solve 3.59, it is possible to make certain assumptions about the system. One assumption is to use the effective mass model (Klimeck, 2004, p. 6), in which case all off diagonal terms $A_{i,j>i}$ and $A_{i>j,j}$ are equal and constant. Here, the constant is denoted by t. The energy can be approximated as

$$E = A_{-2,-2} - 2t\cos(\gamma\Delta), \tag{3.63}$$

where γ is a longtitudal wave vector in the left lead. The GF is then

$$g^{Lr}_{-3,-3} = -\exp(\gamma\Delta)/t, \tag{3.64}$$

which gives the self-energy

$$\Sigma^{r}_{-2,-2} = -t\exp(\gamma\Delta). \tag{3.65}$$

Generally, neighboring blocks will be coupled, so that in the left and right contacts the self-energies respectively are

$$(\Sigma^{in}_{lead})_{i,j} = \sum_{k,l\leq 0} t_{i,k} g^{r}_{k,l} t_{l,j} \tag{3.66}$$

$$(\Sigma^{in}_{lead})_{n,m} = \sum_{k',l'\geq 0} t_{n,k'} g^{r}_{k',l'} t_{l',m}, \tag{3.67}$$

where it should be understood that $i, j \leq 0$ since this self-energy describes the left boundary, and $n, m \geq N-1$ because it describes the right boundary.

3.1.4 Scattering

Scattering events may now be included, so that the governing equations become

$$\left[E - H_0 - \Sigma^r - \Sigma^r_{lead}\right] G^r = 1, \tag{3.68}$$

and

$$\left[E - H_0 - \Sigma^r - \Sigma^r_{lead}\right] G^n = \left[\Sigma^{in} + \Sigma^{in}_{lead}\right] G^a. \tag{3.69}$$

Considering elastic scattering, the self-energies may be expressed as

$$\Sigma^r = D \otimes G^r \tag{3.70}$$
$$\Sigma^{in} = D \otimes G^n, \tag{3.71}$$

where D contains the square of the scattering potential, and $\otimes$ is a convolution over $\boldsymbol{k}$ and orbital indices defined in the beginning of this section. The scattering in/out self-energies for electron-phonon interaction will be discussed below, the other self-energies may be found in appendix B.

Electron-phonon scattering

Let the self-energy Σ^{in}_R denote the scattering self-energy in from the contact to the right, and similarly Σ^{in}_L for the left contact. Then, there will be additional scattering in contribution to the self-energy at energy E from the energy levels above and below. In the Born approximation, it can be argued that the scattering in self-energy will depend on the Bose factor which determines the phonon occupancy, the deformation potential for electron-phonon scattering, and the availability of electrons through the electron correlation GF. Thus, the scattering in self-energy will take the following form (Mahan, 1987, p. 251)

$$\begin{aligned}\left(\Sigma^{in}_{Phonon}\right)_q (E) = \sum_\eta D^\eta_q \Big[& n_B(\hbar\omega_{phonon}) G^n_q(E - \hbar\omega_{phonon}) \\ & + (n_B(\hbar\omega_{phonon}) + 1) G^n_q(E + \hbar\omega_{phonon}) \Big],\end{aligned} \tag{3.72}$$

where $n_B(\hbar\omega_{phonon})$ is the Bose distribution function at energy $\hbar\omega_{phonon}$ for phonons, and D^η_q is the electron-phonon scattering strength or deformation potential at block q. All terms that contribute to the scattering in self-energy is shown in Figure 3.3.

The exact same arguments can be done for the scattering out self-energy, which will take the following form (Mahan, 2000)

$$\left(\Sigma^{out}_{Phonon}\right)_q(E) = \sum_\eta D^\eta_q \Big[(n_B(\hbar\omega_{phonon})+1)G^p_q(E-\hbar\omega_{phonon}) + n_B(\hbar\omega_{phonon})G^p_q(E+\hbar\omega_{phonon})\Big], \tag{3.73}$$

in this case scattering out from a fully filled state.

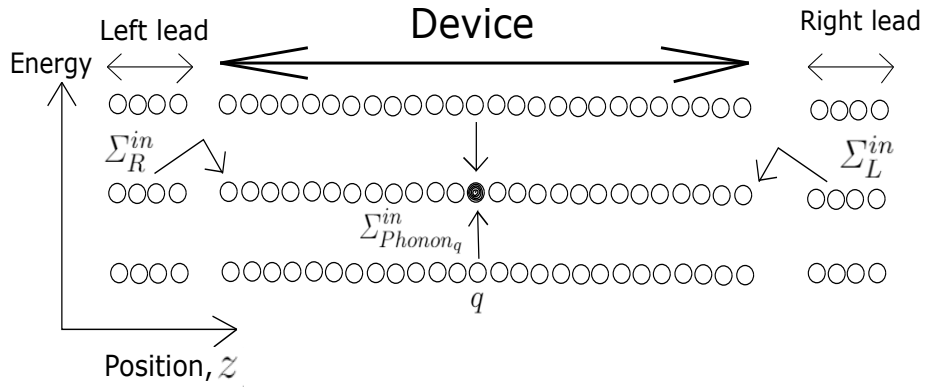

Figure 3.3: Contributions to the scattering in self-energy.

3.1.5 Electron density

The electron density can in the NEGF case be expressed in terms of GFs. The electron density at a position z in the device, will depend on the number of states filled due to the contacts to the left and right. So at block q, the expression will be (M. P. Anantram and Nikonov, 2008, p. 529)

$$n_q(E) = \frac{1}{\pi\Delta}\int \mathrm{d}E\Big[G^r_{q,1}(E)\Sigma^{in}_L(E)G^a_{1,q}(E) + G_{q,n}(E)\Sigma^{in}_R(E)G^a_{n,q}(E)\Big]. \tag{3.74}$$

However, since electron-phonon scattering is present an electron may scatter from a point (q', E') to (q', E), and then propagate to the point (q, E).

So, equation 3.74 must be modified to include this effect as well (M. P. Anantram and Nikonov, 2008, p. 530)

$$\begin{aligned} n_q(E) = \frac{1}{\pi\Delta}\int \mathrm{d}E \Big[& G^r_{q,1}(E)\Sigma^{in}_L(E)G^a_{1,q}(E) \\ & + G_{q,n}(E)\Sigma^{in}_R(E)G^a_{n,q}(E) \\ & + \sum_{q'} G_{q,q'}(E)\Sigma^{in}_{Phonon}(E)G^a_{q',q}(E)\Big]. \end{aligned} \tag{3.75}$$

The contributions are shown in Figure 3.4.

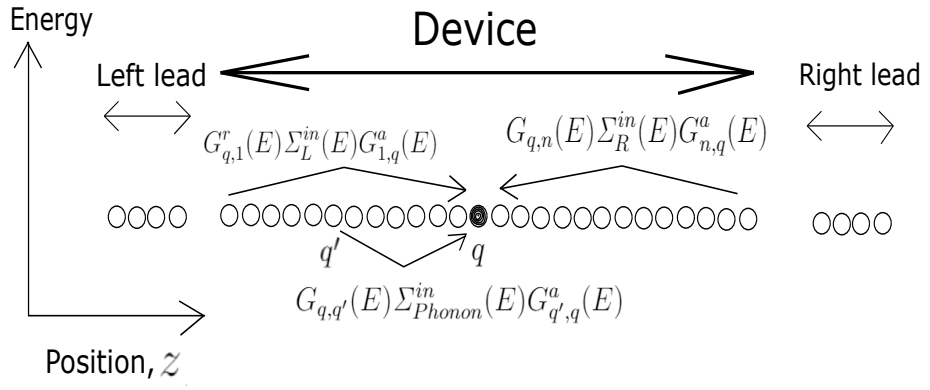

Figure 3.4: All three contributions to the electron density.

Recalling 2.125 and $\Sigma^{in} = \Sigma^{in}_L + \Sigma^{in}_R + \Sigma^{in}_{Phonon}$, the expression for the electron density may be simplified in the following way

$$n_q(E) = \frac{1}{\pi\Delta}\int \mathrm{d}E G^n_{q,q}(E). \tag{3.76}$$

Flowchart

The overall algorithm is depicted in Figure 3.5. As described in subsection 3.1.4, the scattering in/out self-energies respectively depend on the electron/hole correlation GFs. And these GFs again depend on the scattering in/out self-energies. One might then be lead to believe that the entire problem is unsolvable, but by using a few tricks it should be evident that this is not the case.

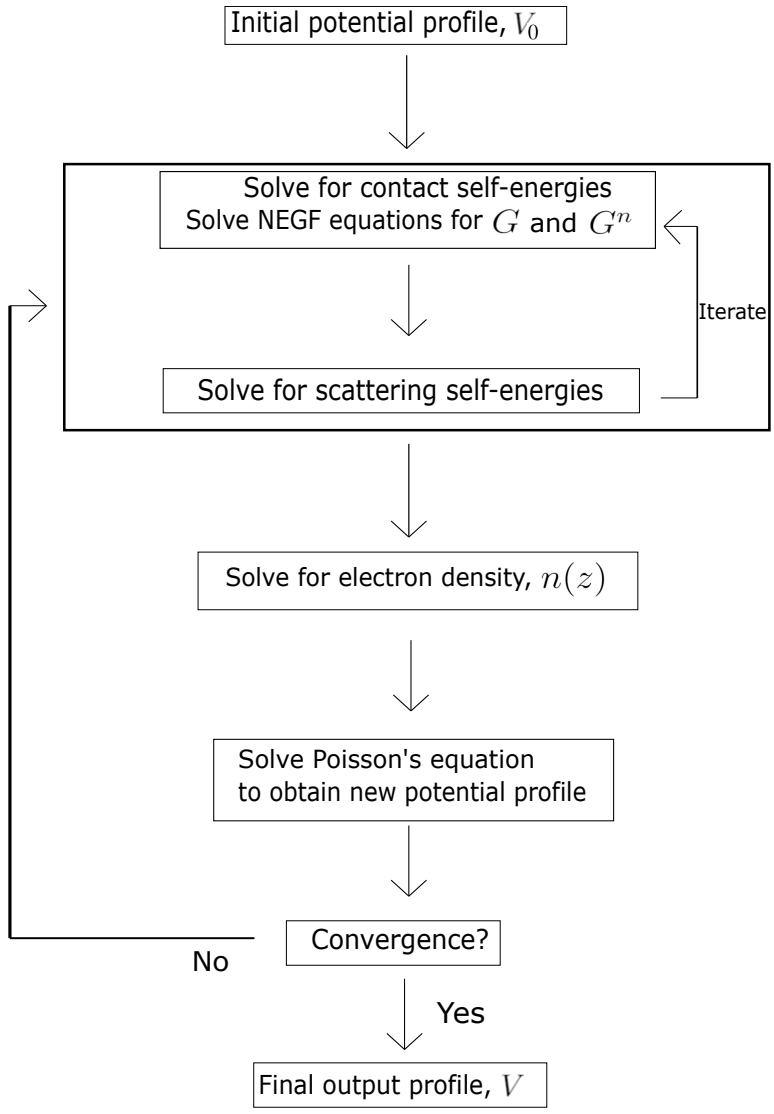

Figure 3.5: The flowchart for the implemented code. It consists of two iterative blocks, see the description below for further details.

It is clear that the conduction band potential profile along with the applied bias V_0 needs to be calculated first, as it is involved in the diagonal part of the Hamiltonian. This, as well as the eigenenergy is used to calculate the retarded and advanced GFs for the structure. In order to solve the electron and hole correlation GFs one may not simply assume that $\Sigma^{in} = \Sigma^{out} = 0$, because this will give $G^n = G^p = 0$ as evident from 2.125 and 2.126.

Instead, one may give another ansatz for the self-energies. Here, the scattering self-energies are assumed to have some constant value not equal to zero. The next step is to use these self-energies in order to calculate the first values for the electron and hole correlation GFs, by using 3.51 and 3.52. Then, these GFs can again be used to calculate new values for the scattering in/out self-energies, by using 3.72 and 3.73. This process just described is the innermost iterative block in Figure 3.5. The ansatz for the scattering in/out self-energies is justified in the sense that if they in fact are zero even though they were assumed to have nonzero values, then after a number of iterations it should be evident that their values do go to zero.

After the iteration process has converged, the program continues to solve for the electron density $n(z)$ by using 3.76. This is then used in the Poisson's equation in order to solve for a new potential profile, which now takes into account bending because of spatial charges. The first time the electron density is calculated, it will be based on the fact that the potential does not take into account any spatial charges. Therefore, the program executes the "no" answer in Figure 3.5 when asked if the potential profile has converged. This leads to calculation of new GFs using the latest potential profile.

This entire process is repeated until convergence of the potential profile has been reached, in which case "yes" is executed and the program yields the final potential profile V.

Chapter 4

Results and discussion

All results have been obtained from a script written by the author in the programming language FORTRAN 95, and MATLAB for plotting. All calculations are based on the material compound $Al_{0.85}Ga_{0.15}As/GaAs$. The lattice temperature is set to $T = 200$ K, and the applied voltage bias is varied between 12 and 50 mV. The simulation time for the SP solver is no more than a few minutes, but the NEGF solver may take up to a few days.

Preliminary results are shown in Figure 4.1. It must be noted that the NEGF method uses a sixth of the grid resolution that is used in the SP calculations, so as to save simulation time. It should also be noted that the results in Figure 4.1 should not be taken as absolute truths, but rather as indicators of how more accurate solutions would look. This is because there are a lot of parameters involved in the calculations which may be adjusted to more accurate values. The bending of the potential profile in Figure 4.1b shows additional bending as a result of the spatial charges.

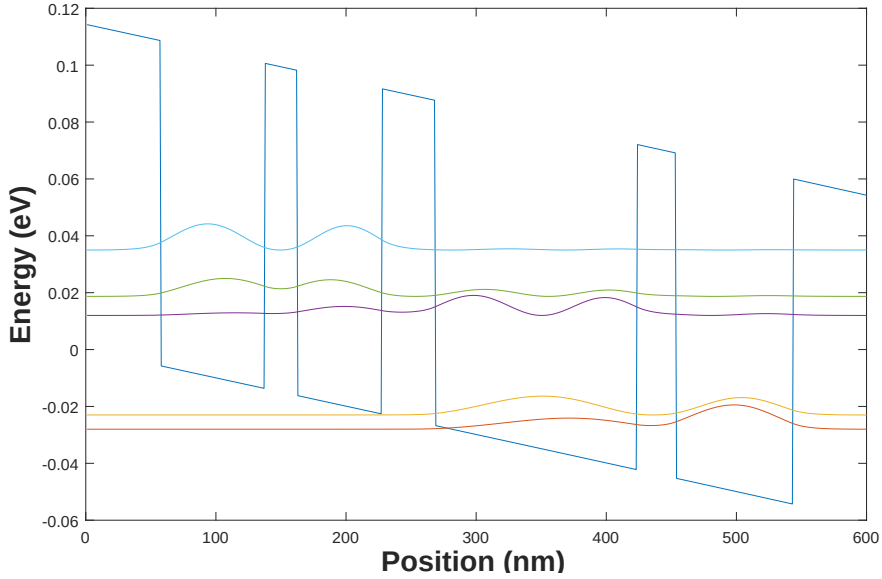

(a) SP results.

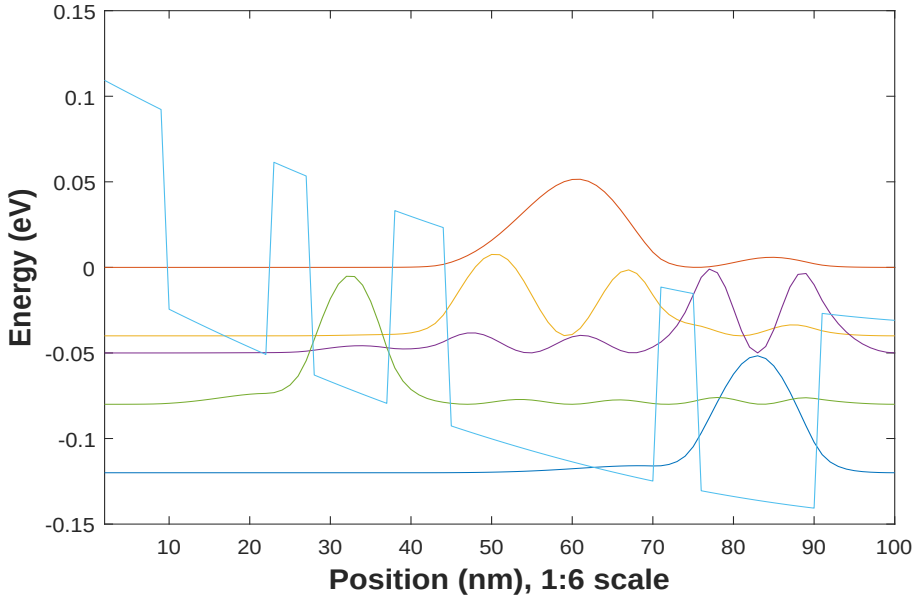

(b) NEGF results.

Figure 4.1: Simulation results, showing five states along with the final potential profile for both cases 4.1a and 4.1b. Both results are simulated at an applied voltage bias of 30 mV.

Figure 4.2 shows further results from the SP simulations. In for instance a QCL or QCD, the eigenstates may be utilized in order to find what wavelengths the device will lase or absorb at. In a QCL, selected states will be filled with electrons which in turn will undergo diagonal optical photon transitions to states with lower energy levels. These states are emptied because extractor states will extract those electrons. The photons emitted in the process will be reflected in a cavity, and eventually give rise to the lasing effect. In a QCD, the process is reversed in the sense that photons are absorbed to excite electrons into higher rather than lower energy eigenstates.

Because the potential profile linearly decreases because of the applied voltage bias, the states will become localized. The reason is that the resonant states in the quantum wells are misaligned as described in Section 2.3, so the probability that an electron will tunnel through one barrier decreases for each barrier. Because each state has a different eigenvalue, they will align with different resonant levels.

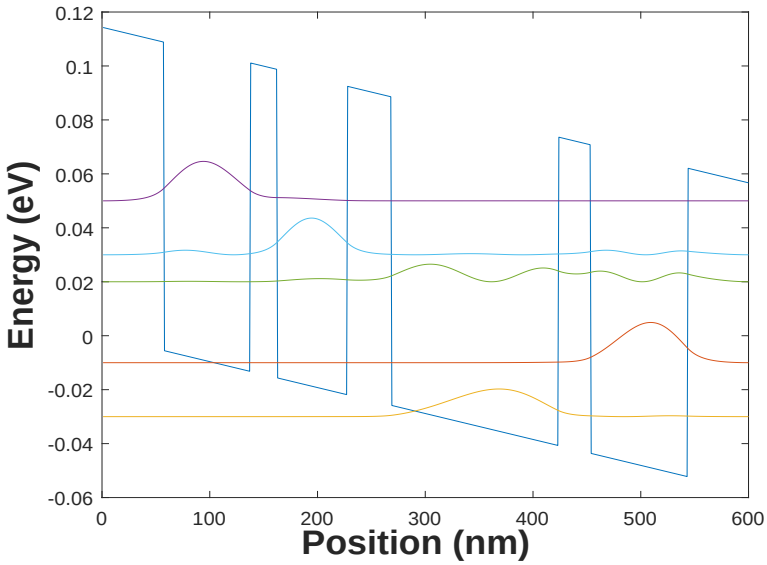

(a) 12 mV applied voltage bias

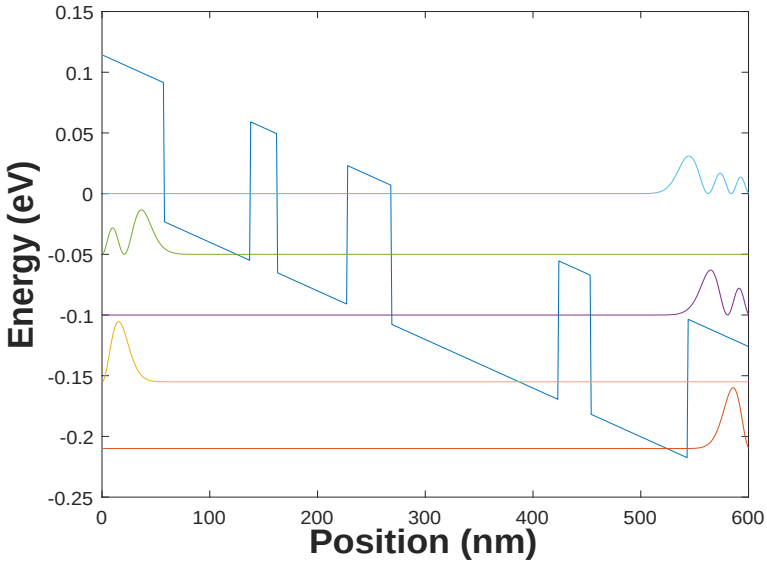

(b) 50 mV applied voltage bias

Figure 4.2: Both Figure 4.2a and 4.2b show the potential profile along with the five first energy eigenstates for two different applied voltage biases.

Chapter 5

Conclusion and outlook

The SP solver provides a simple and fast way of studying layered devices such as the system described in this report. However, it is not nearly accurate enough, as one has to assume an expression for the electron density. It does not take into account inelastic or electron-phonon scattering effects. Nor does it take in the fact that during scattering events in nanoscale devices, electrons will be affected by the applied voltage bias. In fact, scattering events cannot be taken as changes along the electron's path, because the path doesn't exist (Jacoboni, 2010, p. 335).

Using instead the NEGF approach, the electron density may immediately be expressed through GFs. Now, both elastic and inelastic effects are taken into account. But for a high price, because the solution very slowly converges. This is even after simplifying the discretized expressions of the GFs, so that they are not calculated in their full matrix forms. Thus, current research is focused on what quantum effects are relevant for accurate calculations while balancing computational time. So, one method is to is to implement aspects of quantum transport into the semiclassical transport theory. In this way, computational time is optimized, while simultaneously giving an accurate picture of the quantum transport theory. For instance, a hybrid of the NEGF and Monte Carlo approaches is considered. In this way, resonant tunneling is treated in some regions for instance through a thick barrier by the NEGF approach, but the rest of the device is simulated using the semiclassical transport theory.

Another method that the author will suggest, is to use a proof-of-work system (Investopedia, 2018). By doing this it should be possible to avoid

simulation times of full matrices of several years. Since the main contributor to the simulation time is matrix inversions, it is possible through proof-of-work to distribute these tasks on a network of participants. Each participant will solve a small part of the problem, and send the solution back to the host for verification. Given that the solution is correct, the host will provide a new problem for the participant again. The incentive to participate is to be rewarded with some currency or coin. It should be noted that this solution is fairly new with few implementations, but it has been shown to work and could prove to solve the great challenge of slow NEGF simulations (R. Heart and Mesquita, 2017).

Bibliography

Cassan, E., 2000. On the reduction of direct tunneling leakage through ultrathin gate oxides by a one-dimensional schröodinger-poisson solver. J. Applied Phys. 87 (11), 7931–7939.

D. Hofstetter, F.R. Giorgetta, E. B. Q. Y. C. M., Köhler, K., 2010. Mid-infrared quantum cascade detectors for applications in spectroscopy and pyrometry. Applied Physics B : Lasers and Optics 15 (2), 313–320.

D. Vasileska, S. M. G., Klimeck, G., 2010. Computational Electronics. Taylor and Francis Group, LLC.

Franckié, M., 2016. Modelling Quantum Cascade Lasers. Lund University.

H. Li, J. C. C., Liu, H. C., 2008. Effects of design parameters on the performance of terahertz quantum-cascade lasers. Semicond. Sci. Technol. 23 (12), 125 04016.

Hashimura, K., Ishii, K., Akikusa, N., Edamura, T., Yoshida, H., Awazu, K., 2014. Coagulation and ablation of biological soft tissue by quantum cascade laser with peak wavelength of 5.7 μm. Innovative Optical Health Sciences 7 (3), 1450029.

Investopedia, L., 2018. Proof of work. `https://www.investopedia.com/terms/p/proof-work.asp`.

J. Faist, F. Capasso, D. L. S. C. S. A. L. H., Cho, A. Y., 1994. Quantum cascade laser: A new optical source in the mid-infrared. Proceedings of the Sixth International Conference on Infrared Physics 36 (1), 99–103.

Jacoboni, C., 2010. Theory of electron transport in semiconductors. Springer-Verlag Berlin Heidelberg.

Jirauschek, C., 2009. Accuracy of transfer matrix approaches for solving the effective mass schröodinger equation. IEEE J. Quantum Electron 45 (9), 1059–1067.

Jirauschek, J., Kubis, T., 2014. Modeling techniques for quantum cascade lasers. Applied Physics Reviews 1 (1), 011307 – 1–51.

Klimeck, G., June 14 2004. Numerical aspects of negf: The recursive green function algorithm. https://nanohub.org/resources/165.

M. P. Anantram, M. P. L., Nikonov, D. E., 2008. Modeling of nanoscale devices. Proceedings of the IEEE 96 (9), 511–550.

Mahan, G. D., 1987. Quantum transport equation for electric and magnetic fields. Physics Reports 145 (5), 251–318.

Mahan, G. D., 2000. Many-Particle Physics. Springer.

Ming-Yang Li, Chang-Hsiao Chen, Y. S., Li, L.-J., 2008. Heterostructures based on two-dimensional layered materials and their potential applications. Semicond. Sci. Technol. 19 (6), 322–335.

R. Heart, D. B., Mesquita, K., 2017. Technology overview. https://cfdtoken.com/pdf/core_tech.pdf.

Shafer, T. R., 2009. Three pictures of quantum mechanics. https://uncw.edu/phy/documents/Shafer_09.pdf.

Shockley, W., 1950. Electrons and Holes in Semiconductors. Van Nostrand Reinhold Inc., U.S.

Singh, J., 2003. Electronic and optoelectronic properties of semiconductor structures. Cambridge University Press.

Appendix

A Derivation of 3.49

Equation 3.49 is derived by using 3.44

$$g^{Ln}_{i,i} = (g^{r}_{i,i})_0 A^{\dagger}_{i,i-1} g^{Ln}_{i-1,i} + (g^{r}_{i,i})_0 \Sigma^{in}_{i,i} g^{La}_{i,i} + (g^{r}_{i,i})_0 \Sigma^{in}_{i,i-1} g^{La}_{i-1,i}. \quad (1)$$

Equation 3.46 can be used in order to express $g^{Ln}_{i-1,i}$ by known quantities

$$g^{Ln}_{i-1,i} = (g^{Ln}_{i-1,i})_0 + (g^{Ln}_{i-1,i})_0 A^{\dagger}_{i,i-1} g^{La}_{i-1,i} - g^{Ln}_{i-1,i-1} A^{\dagger}_{i-1,i} g^{La}_{i,i} - g^{Lr}_{i-1,i-1} A_{i-1,i} g^{Ln}_{i,i}. \quad (2)$$

Substituting this into Equation 1 gives

$$\begin{aligned} \big[I - (g^{r}_{i,i})_0 A_{i,i-1} g^{Lr}_{i-1,i-1} A_{i-1,i}\big] g^{Ln}_{i,i} \\ = (g^{r}_{i,i})_0 \Sigma^{in}_{i,i} g^{La}_{i,i} + (g^{r}_{i,i})_0 \Sigma^{in}_{i,i-1} g^{La}_{i-1,i} \\ -(g^{r}_{i,i})_0 A_{i-1,i} \big[(g^{Ln}_{i-1,i})_0 + (g^{Ln}_{i-1,i})_0 A^{\dagger}_{i,i-1} g^{La}_{i-1,i} \\ - g^{Ln}_{i-1,i-1} A^{\dagger}_{i-1,i} g^{La}_{i,i}\big], \end{aligned} \quad (3)$$

and using

$$(g^{Ln}_{i,i+1})_0 = g^{Lr}_{i,i} \Sigma^{in}_{i,i+1} g^{La}_{i+1,i+1} \quad (4)$$

$$(g^{Ln}_{i+1,i})_0 = g^{Lr}_{i+1,i+1} \Sigma^{in}_{i+1,i} g^{La}_{i,i}, \quad (5)$$

the following is obtained

$$\begin{aligned} g^{Ln}_{i,i} = g^{L} r_{i,i} \big[\Sigma^{in}_{i,i} - A_{i-1,i} g^{Ln}_{i-1,i-1} A^{\dagger}_{i-1,i}\big] g^{La}_{i,i} \\ + g^{Lr}_{i,i} \Sigma^{in}_{i,i-1} g^{La}_{i-1,i} - g^{Lr}_{i,i} A_{i-1,i} g^{Lr}_{i-1,i-1} \Sigma^{in}_{i-1,i} g^{La}_{i,i}. \end{aligned} \quad (6)$$

Noting that $g^{Lr}_{i,i-1} = g^{Lr}_{i,i} A_{i-1,i} g^{Lr}_{i-1,i-1}$, 3.49 should follow immediately.

B Self-energies

Phonons

These are the expressions for the scattering in phonon self-energies, where the deformation potential is specified

$$\Sigma^{in}_{\alpha,L,\alpha',L'}(k,E) = \frac{1}{V}\sum_{\boldsymbol{q}} \left|U_{\boldsymbol{k}-\boldsymbol{q}}\right|^2 \exp(iq_z\Delta(L-L'+\nu_{\alpha,\alpha'})) \times \big[n_{\boldsymbol{q}} G^n_{\alpha,L,\alpha',L'}(\boldsymbol{q}_t; E-\hbar\omega_{\boldsymbol{q}}) + (n_{\boldsymbol{q}}+1) G^n_{\alpha,L,\alpha',L'}(\boldsymbol{q}_t; E+\hbar\omega_{\boldsymbol{q}})\big], \quad (7)$$

and

$$\Sigma^{in}_{\alpha,L,\alpha',L'}(k,E) = \frac{1}{V}\sum_{\boldsymbol{q}} \left|U_{\boldsymbol{k}-\boldsymbol{q}}\right|^2 \exp(iq_z\Delta(L-L'+\nu_{\alpha,\alpha'})) \times \big[(n_{\boldsymbol{q}}+1) G^n_{\alpha,L,\alpha',L'}(\boldsymbol{q}_t; E-\hbar\omega_{\boldsymbol{q}}) + n_{\boldsymbol{q}} G^n_{\alpha,L,\alpha',L'}(\boldsymbol{q}_t; E+\hbar\omega_{\boldsymbol{q}})\big], \quad (8)$$

where U is the Fourier transformed scattering potential, $n_{\boldsymbol{q}}$ is the electron density for mode $\boldsymbol{q}$, α run over anion and cation states, L is the length to a layer of cations, and finally ν is defined as

$$\nu_{\alpha,\alpha'} = \begin{cases} 1/2 & \text{if } \alpha = a, \alpha' = c \\ -1/2 & \text{if } \alpha = c, \alpha' = a \\ 0 & \text{otherwise} \end{cases}. \quad (9)$$

Alloy disorder

From the potentials V_A and V_B in subsection 2.2.3, one may define $\delta V(\boldsymbol{r}) = V_A(\boldsymbol{r}) - V_B(\boldsymbol{r})$. Given a matrix element $M_{\alpha,\alpha'} = \langle \alpha | \delta V(\boldsymbol{r}) | \alpha' \rangle$, the alloy self energy may be written as

$$\Sigma^{in}_{c,L,c',L'} = \frac{2\Delta^2 x(1-x) M_{c,L,c',L'} M_{c',L',c,L}}{A} \times \sum_{\boldsymbol{q}} G^n_{c,L,c',L'}(\boldsymbol{q}), \quad (10)$$

where A is the cross sectional area described earlier.

Interface roughness

This self-energy becomes

$$\Sigma^{in}_{c,L,c',L'} = \frac{x(1-x)M_{c,L,c',L'}M_{c',L',c,L}}{A} \times \sum_{\boldsymbol{q}} \left|U_{\boldsymbol{k}-\boldsymbol{q}}\right|^2 G^n_{c,L,c',L'}(\boldsymbol{q}). \tag{11}$$

Ionized impurities

Fourier transforming the screening potential in 2.19, one may obtain the generalized self-energy

$$\Sigma^{in}_{\alpha_1,L_1,\alpha_2,L_2}(\boldsymbol{k}) = \frac{e^4}{8A\varepsilon^2}\sum_L n_s^L \times \sum_{\boldsymbol{q}} \frac{\mathrm{e}^{-\sqrt{q_0^2+\left|\boldsymbol{k}-\boldsymbol{q}\right|^2}\left[\left|L_1-L\right|+\left|L_2-L\right|\right]\Delta}}{q_0^2+\left|\boldsymbol{k}-\boldsymbol{q}\right|^2} \times G^n_{\alpha_1,L_1,\alpha_2,L_2} \tag{12}$$